USC University of Southern California

Team AirSCailors
AirSChooner-105 P/C

AIAA Undergraduate Individual Aircraft Design

David Moeller Sztajnbok

May 2023

David Moeller Sztajnbok

Name	AIAA Number	Signature
David Moeller Sztajnbok	**1255637**	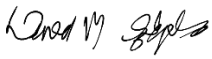

Faculty Advisor	AIAA Number	Signature
Dr. Geoffrey R. Spedding	**233796**	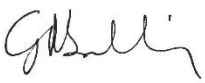

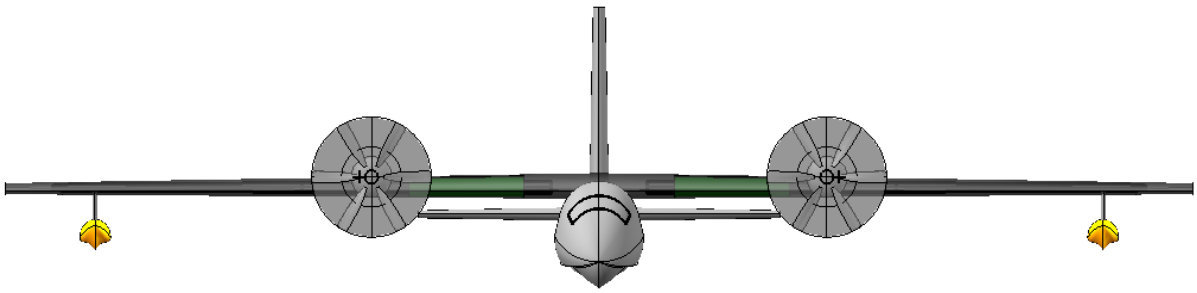

Acknowledgements

A (huge) special thanks to:

Dr. Geoffrey R. Spedding for accepting so promptly to guide me through this project and for introducing me to (and keeping me interested in) the beautiful science that is Aerospace Engineering

And to:

Dr. Michael Kruger for the incredible help and crucial support throughout the report, particularly with OpenVSP, drawings, sizing, layouts, and all-things design related

Table of Contents

List of Figures

List of Tables

Chapter 1 – Introduction

1.1 Executive Summary

This report will show the sizing, design, and analysis of an amphibian aircraft tailored for short range missions capable of STOL in land and water environments. The aircraft is to enter service in 2031, with production beginning as early as 2026.

This report will show that the design converged in a high-wing, conventional aircraft configuration powered by two turboprops mounted in pods on the wings. Wingtip floats support the weight of the aircraft on water landings, and a composite-built hull offers the required hydro stability for water missions.

This report will also show the layout process of the aircraft, including reasoning and calculations for internal volume and demonstrations of the fitting of said internal volumes. Weights & Balance, Aerodynamics, and Stability & Control were considered at every step of the layout process, and the analysis of each category cited above confirms the feasibility of the aircraft.

1.2 Requirements Introduction

This year's RFP calls for the design of a "New Efficient Water and Terrestrial (NEWT)" aircraft. It is to be an amphibious, multi-mission capable aircraft. The aircraft must be able to fly a design passenger mission, an economic passenger mission, and a cargo mission.

The motivation behind the RFP is the entry into the market of air passenger and cargo commerce following and aiding in the development of outlying communities and developing countries, where airports might offer less infrastructure, shorter runways, and other challenges. Particularly, island communities would benefit from an aircraft optimized for amphibious capabilities, since the main aircraft that serve this purpose are not amphibious by nature, but rather have the capability to carry out water missions with the installation of floats.

It is with this goal in mind – the development of an amphibious, multi-mission, rough and short terrain capable aircraft – that the design was carried out.

1.3 Requirements Overview

The RFP[1] lays out some general requirements. The aircraft must be able to take off and land from runways as well as both fresh and salt water. It has a minimum cruise speed of 200 kts and a target cruise speed of 250+ kts. It must be VFR and IFT capable, be able to fly in icing conditions, be FAR 23 compliant, and demonstrate better energy cost per passenger than competition. It must also be in service by 2031. Note that the target cruise speed of 250+ knots is a tradeable requirement, while a cruise speed of at least 200 knots is a mandatory requirement. This is addressed in the next chapter.

The RFP also lays out the following mission-specific requirements, generally related to take-off and landing field lengths, ranges, and weight:

Table 1-1: Summary of mission-specific requirements

Requirement Type	Design Passenger Mission	Economic Passenger Mission	Cargo Mission
Payload	1 flight crew + 19 passengers	1 flight crew + 19 passengers	5000 lbs
Range	250 nmi	150 nmi	200 nmi
Take-Off and Landing Considerations	<= 1500 ft over 50’ obstacle to runway with dry pavement <= 1900 ft on water over a 50’ obstacle Ability to take-off and land in Sea State 3 conditions	-	-
Additional/Miscellaneous	28’’ or greater seat pitch Passenger weight of 193.6 lbs Baggage weight of 37.4 lbs, volume of 4 ft^3	*Same as design passenger*	-
Flying Qualities	CFR Part 23	CFR Part 23	CFR Part 23

It is worth noting that take-off and landing performance must be demonstrated at 5000’ MSL and, in the case of the use of a runway, performance must be demonstrated for dirt, grass, metal mat, gravel, asphalt, and concrete fields.

Lastly, it is also worth noting that this aircraft is expected to enter service (that is, EIS date) in 2031. The general requirements specify that this assumption can be used for the powerplant but will be used for technology in general. One example might be a correction factor for avionics weight. These factors will, of course, be kept to a minimum and be quite conservative, but the reader should keep an eye out for the “2031 EIS” justification.

Each of these requirements will be revisited after the design is complete.

1.4 Analysis of Competition

It is important to assess the main competitors of the amphibious aircraft market to identify design points, trends, and for increased awareness in general during the design process.

Below are tables with data from competitive aircraft designs. These are all specified in the RFP as potential competitors. The tables are split between performance and geometry values. The data below will be used to assess the similarity of our to-be-designed aircraft with existing ones, which can guide the selection of design points such as wing loading, thrust-to-weight ratio, aerodynamic features, and many others.

Table 1-2: Performance summary of competitive aircraft

Parameter	ShinMaywa US-2	Beriev Be-200	Bombardier 415	Twin Otter	Caravan Amphibian
MTOW [lb]	105,160	90,389 (land) 83,775 (water)	41,000 (land) 37,850 (water)	12,500	8,000
Max Fuel Weight [lb]	38,620	27,025	10,250	-	2,224
Max Payload Weight [lb]	-	16,534	13,500	4,280	-
Empty Weight [lb]	56,504	60,848	30,000	6,881*	4,980
W/S [lb/ft^2]	67.85	74.99	35.05	29.76	28.63
W/P [lb/shp]	6.97	-	7.95	-	11.85
W/T [lb/lbf]	-	2.86	-	-	-
Max Cruise Speed [kts]	259 (FL 200)	378 (FL262)	197 (FL100)	182 (FL100)	162 (FL100)
Stall Speed No Flaps [kts]	-	116	-	74	74
Stall Speed Flaps [kts]	-	84	80	58	59
Take-Off Field Length [ft] (35ft clearance)	2,150 (land) 1,820 (water)	4,170 (land) 3,280 (water)	2,770 (land) 2,670 (water)	1,200	1,100 (land) 1,920 (water)
Landing Field Length [ft] (50 ft clearance)	2,655 (land) -	3,350 (land) 4,265 (water)	2,200 (land) 2,180 (water)	1,050	1,490 (land) 1,935 (water)
Range Max Freight [nm]	2537	540	1310	775	790

Table 1-3: Geometry summary of competitive aircraft

Parameter	ShinMaywa US-2	Beriev Be-200	Bombardier 415	Twin Otter	Caravan Amphibian
Wing Area [ft^2]	1,462	1,264.2	1,080	420	279.4
Wing Aspect Ratio [-]	8.1	9.1	8.2	10.1	9.7
Wing Chord [ft]	-	18.29 (root) 5.64 (tip)	11.62 (constant)	6.5 (constant)	6.5 (root) 4.0 (tip)
Vertical Stab. Area [ft^2]	-	135.63	120.75	48	38.41
Vertical Stab. Span [ft]	-	-	-	-	-
Horizontal Stab. Area [ft^2]	248	193.33	221.2	100	70.04
Horizontal Stab. Span [ft]	40.7	33.19	36	20.66	20.5
Fuselage Length [ft]	109	95.75	65	49.5	38.9
Fuselage $Diameter_{max}$ [ft]	-	9.375	-	-	-
Length-to-Beam Ratio [-]	-	-	7.5	-	-

It is worth noting that some of these aircraft, such as the Beriev Be-200, fly not only passenger and cargo missions but also other types of missions. In the case of the Be-200, firefighting missions. In these cases, values for maximum weights, loadings, etc. are taken for the freight mission. Also worth noting that these values were taken from [2]. Whenever a parameter was not given but could be estimated based on the numbers given, an estimation was made with special attention to weights and areas used as reference.

1.5 Conclusions and Design

From the analysis of the aircraft above, it is possible to conclude that there is space in the market for an aircraft of the specifications laid out in the RFP. Most aircraft from the list are either too heavy (as will be concluded in the next chapter) or have higher ranges, indicating that the purpose of the to-be-designed NEWT is not fully serviced by the aircraft available. Specifically, a moderate weight, short range, fully amphibian aircraft is not fully described by the options.

Although aircraft like the US-2 are in a completely different weight category than the to-be-designed NEWT, many specific design choices can be observed and kept in mind. It is of great importance that the aircraft is

fully amphibian. Aircraft like the Caravan Amphibian or the Twin Otter 400, though likely capable of a similar mission as the one in the RFP, cannot be considered fully amphibian aircraft. They use large, exchangeable floats mounted off the sides of the bottom of the fuselage, as shown in the image below.

Instead, a design more similar to the US-2, Be-200, and Seastar will be adopted here. The fuselage serves as a hull where the landing gears are retracted into, allowing both land and water operations with the same airframe. Another design choice noted in the US-2 and Be-200 is the presence of large floats on the wing tips to maintain the aircraft above the water ("hydrostability" in roll). These must be carefully considered and will be approached in detail later.

Chapter 2 - Initial Sizing

2.1 Introduction

In this chapter, three crucial parameters for the aircraft are determined: take-off gross weight W_{TO}, aircraft empty weight W_e, and fuel weight W_f. These values will later be used to determine a variety of different parameters, namely wing loading and power loading, as well as sizing a variety of different components.

2.2 Summary of Sizing Method

A summary of the sizing method utilized is presented below.

The method of weight fractions was used for initial sizing. This method is described in detail in books like Raymer[3] and Roskam[4]. This author has chosen to follow more closely the methods in Raymer.

Take-off gross weight is determined by the equation below:

$$W_0 = \frac{W_{crew} + W_{payload}}{1 - \frac{W_f}{W_0} - \frac{W_e}{W_0}} \qquad 2.1$$

Where W_{crew} and $W_{payload}$ are, respectively, crew weight and payload weight. Also, W_f/W_o is the fuel weight fraction, a fraction of take-off gross weight, and W_e/W_o is empty weight fraction, also a fraction of take-off gross weight.

Note that two terms, fuel weight fraction and empty weight fraction, are functions of take-off gross weight. Therefore, an iterative process is required. In this process, a guess of W_0 is made, then the value of W_0 is calculated, and the two compared. If they differ, a value between the two is selected, and the process is repeated with the new guess. Once they reach a certain proximity, the process is finalized and W_0, W_e, and W_f are found.

In Raymer, W_f/W_o is determined by the method of fuel fractions, described below. W_e/W_o is found by means of a statistical method. The iteration of the method was made automatic using custom MATLAB scripts written by

this author. These scripts were validated by replicating sizing examples in Raymer and Roskam and have presented reasonable results with acceptable accuracy.

On a last note, the aircraft must be designed for three different design missions. This design will assume the same airframe for all missions. This implies a constant empty weight. Therefore, the sizing can be conducted separately for each mission by changing the crew and payload weight, as well as fuel weight, the latter of which being influenced by range and endurance requirements. There is a small caveat to this: empty weight is determined iteratively as a function of take-off weight. Therefore, empty weight is initially sized for the main, passenger mission, and then held constant for the cargo and economic passenger missions.

2.3 Mission Profile and Relevant Assumptions

One example of mission profile to be used in sizing is displayed below. Values for range and loiter are given in the RFP and vary from mission to mission:

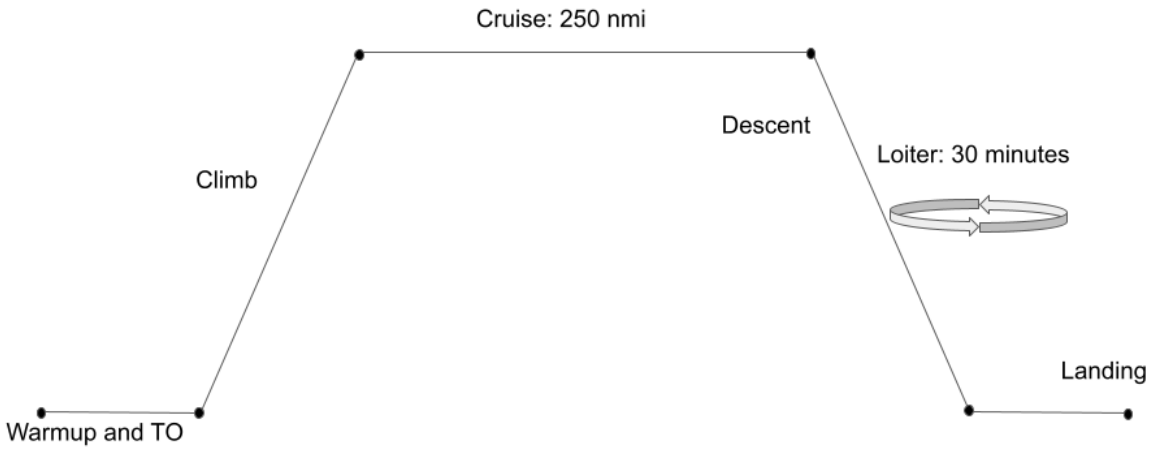

Figure 2.1: Design passenger mission profile example

Values for cruise altitude are not specified in the RFP. An appropriate, preliminary value for the service ceiling is thus selected as FL250 with pressurization limitations in mind. The ranges specified in the RFP are quite low, so such altitude is an appropriate choice with weight as a measure of merit in mind (pressurization systems increase structural weight).

Cruise speed is specified as a tradable value in the RFP. For initial sizing, the value of 250kts is selected. Trade studies will be conducted later in this chapter.

Crew and payload weight are also specified in the RFP. This author will assume 3 crew members for passenger missions, and 2 crew members for cargo missions. The value W_{crew} + $W_{payload}$ in eq. (2.1) is thus estimated with the human and baggage weight in the RFP.

Lastly, assumptions regarding specific fuel consumption and the powerplant were made. Given the mission profile, namely the low cruise speeds and altitudes, the choice of a propeller-driven engine is ideal. Typical values of specific fuel consumption were selected and calculated using the methods in Roskam[4], and are typically range around 0.4-0.5.

2.4 Empty Weight Fraction Determination

Empty weight, W_e, is determined by statistical means following the method in Raymer[3].

The empty weight fraction can be approximated statistically by using the following empirical formula:

$$\frac{W_e}{W_0} = A{W_0}^B \qquad 2.2$$

Where *A* and *B* are statistical fitting constants that vary according to aircraft type. A table of values for *A* and *B* are found in Raymer[3]. For flying boats, they are, respectively, *1.09* and *-0.05*. Empty weight fraction can therefore be expressed as:

$$\frac{W_e}{W_0} = 1.09{W_0}^{-0.05} \qquad 2.3$$

And will be found iteratively in the passenger design mission, then held constant for the other missions.

2.5 Fuel Weight Fraction Determination

To determine fuel weight, the method of mission segment weight fractions, described in many books, including Raymer[3] and Roskam[4], was used.

In the present method, the mission profile as shown in Figure 2.1 is broken down into segments numbered 0 to n, where n is the last point (generally landing and perhaps taxi to gate/stopping point). The weight at the end of segment *i* is given by:

$$\frac{W_{i+1}}{W_i}$$

In other words, W_i indicates the weight at the beginning of segment *i*. Therefore, by multiplying all weight fractions together, we get the ratio between the final and the initial weight, often denoted W_{ff}.

The fuel weight fraction is therefore given by the expression below:

$$\frac{W_{fuel}}{W_0} = 1.06(1 - W_{ff}) \qquad 2.4$$

Where W_{ff} is the ratio between final weight and initial weight. By subtracting that from one, we get how much weight was lost during the mission, in this case due to fuel consumption. A multiplier of 6% is used to account for reserves and trapped fuel.

Note an important assumption here: no weight is lost other than fuel burned. Therefore, no payload was dropped. This is not a problem for this mission – we don't expect to lose weight other than due to fuel burn in either passenger missions or cargo missions – but for other applications such as military fighters, where bombs may be dropped, this must be considered.

2.5.1 L/D Estimation

Lift-to-drag ratio is a measure of an aircraft's aerodynamic efficiency, and is crucial for calculations involving performance, aerodynamics, and much more. It is also of crucial importance during initial sizing. Because the aircraft is not fully drawn yet, a method for estimating L/D must be used. The method described in Raymer[3] is employed below and summarized in the following equation:

$$\left(\frac{L}{D}\right)_{max} = K_{LD}\sqrt{\frac{AR}{\frac{S_{wet}}{S_{ref}}}} \qquad 2.5$$

Above, K_{LD} is a constant, taken as 11 as suggested in Raymer for this type of aircraft. The wetted area ratio, S_{wet} / S_{ref} is approximated by data from historical aircraft. Based on the competition analyzed in Chapter 1, this ratio is taken as 7. Aspect ratio is also assumed to be 10, reasonable for this type of aircraft.

The maximum lift-to-drag ratio is therefore found to be:

$$\left(\frac{L}{D}\right)_{max} = 13.1$$

Which is reasonable compared to historical data in Raymer.

2.5.2 Specific Fuel Consumption Assumptions and Breguet Equations

The last item needed in the estimation of fuel weight is data on specific fuel consumption (SFC), or how much fuel the engine burns. This assumption must be made with caution, since it heavily relies on the type of engine used. Luckily, the requirements for this RFP are very indicative of a prop-driven engine due to the low range and loiter requirements. A jet engine, which consumes more fuel, is more complex, and can be heavier, is not worth the complexity.

Therefore, this author assumes the use of a propeller-driven engine, either a piston-prop or turboprop. Powerplant selection will be later discussed. Propeller-SFC is estimated based on the assumption of a brake horsepower SFC, or C_{bhp}. We assume the following values for SFC based on data in Raymer's table 3.4:

$$C_{bhp,cruise} = 0.5 \frac{lb}{(bhp)(hr)}$$

$$C_{bhp,loiter} = 0.6 \frac{lb}{(bhp)(hr)}$$

We can now estimate the fuel consumed using the following equations, known as the Breguet (range and loiter) equations:

Cruise

$$\frac{W_i}{W_{i-1}} = e^{\frac{-RC}{V(\frac{L}{D})}} \qquad 2.6$$

Loiter

$$\frac{W_i}{W_{i-1}} = e^{\frac{-EC}{\frac{L}{D}}} \qquad 2.7$$

Where *R* is the segment's range requirement (in nautical miles) and *E* is the segment's loiter requirement (in minutes, usually.) The units are all converted to *ft* and *s* for computations in the code.

2.6 Calculation of W_0

The process to compute take-off weight is iterative. A guess for W_0 is made. The value of payload weight is known or estimated by information in the RFP. The empty weight fraction is estimated statistically as mentioned above, and the fuel weight fraction is determined by stepping through the mission profile segments and estimating their weight fractions, also explained above.

Finally, with all these fractions computed based on our assumption of W_0, we compute a value for W_0 using eq. 2.1 and compare our guess to this calculated value. If the numbers are close enough, we have a value for W_0. If not, the guess is changed, and the process repeated.

This author has written a MATLAB code to speed this process. The code was validated using examples found in Raymer and Roskam[3,4]. The following is the last few output lines of the code from the design passenger mission:

```

*SIZING ITERATIONS*

---

*ITERATION 11 -> W0 Guess: 21619.51 | W0 Calculated: 21618.66 | Percentual Difference: 0.00004*

*%%%%%%%%%*

*ITERATION 12 -> W0 Guess: 21619.08 | W0 Calculated: 21618.72 | Percentual Difference: 0.00002*

*%%%%%%%%%*

*ITERATION 13 -> W0 Guess: 21618.90 | W0 Calculated: 21618.74 | Percentual Difference: 0.00001*

*%%%%%%%%%*

```

Therefore, W_0 value is set as 21,619 lbs. The empty weight fraction was determined to be roughly 66% of W_0, such that the empty weight is determined to be 14,306 lbs. This value will be held constant through the other missions.

For the cargo and economic passenger missions, a similar process was repeated. The code was modified to account for changes in payload weight, range, and loiter requirements. A table showing a summary of the calculated weights is displayed below:

Table 2-1: Initial Sizing Values

	Design Passenger Mission	Design Cargo Mission	Economic Passenger Mission
Empty Weight	14,306 lbs	14,306 lbs	14,306 lbs
Payload Weight	5,082 lbs	5,462 lbs	4,851 lbs
Fuel Weight	2,231 lbs	2,104 lbs	1,875 lbs
Take-off Weight (W_o)	21,619 lbs	21,872 lbs	21,032 lbs

This concludes the initial sizing. A more refined method will be used after we know our wing and powerplant characteristics with more detail. For that, values for *W/S* and *T/W* (or *P/W*) must be selected, which will be done in the following chapter.

2.7 Cruise Velocity Trade Study

To confirm the sensitivity to cruise velocity, the sizing was repeated for a range of cruise velocities. The result is shown in the figure below:

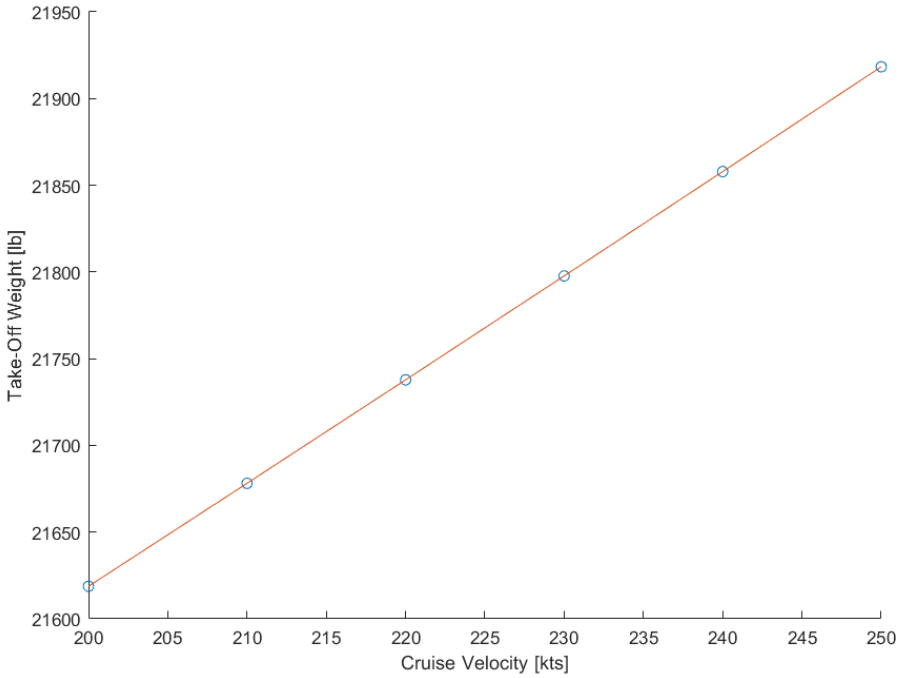

Figure 2.2: Take-off Weight vs. Cruise Velocity

The difference in weight is not significant. This will become clear when more involved weight estimates are made, but 200 lbs does not affect initial sizing considerably. Thus, the choice to continue with 250 kts as the target cruise speed is confirmed.

Chapter 3 –Wing Loading and Power-to-Weight Ratio

3.1 Introduction

In this chapter, the aircraft's wing loading and power-to-weight ratio are selected by using the method of thrust matching. Thrust matching consist of calculating a variety of values for wing loading constrained by different performance parameters, such as stall speed, take-off and landing rolls, turn performance, etc. and selecting the most conservative of these values. A value for power-to-weight ratio is selected using Raymer's statistical approach, but subsequent values of wing loading are calculated using the performance constraints.

3.2 Power-to-Weight Ratio Selection

P/W can be calculated statistically with the equation below:

$$\frac{P}{W_0} = \alpha V_{max}^{C} \qquad 3.1$$

Where α and C are determined statistically to be:

$$\frac{P}{W_0} = 0.03\, V_{max}^{0.23}$$

Using our value of V_{max} to be the conservative 250 kts, and converting it to ft/s, we arrive at an initial value for power loading:

$$\frac{P}{W_0} = 0.12 \frac{\text{hp}}{\text{lb}}$$

Which is similar to the typical value for power-to-weight ratio in Raymer for seaplanes, a good sign.

Note that this is the P/W at take-off conditions, that is, referencing design take-off weight. As fuel is burned, P/W increases. Power-to-weight ratio is thus dependent on the phase of flight due to the weight change caused by fuel burn.

3.3 Powerplant and Thrust Matching

From now on, this author assumes the use of a turboprop engine. This will be justified more thoroughly later but is a very natural decision due to the range and speed requirements, as well as analysis of competition.

The power-to-weight ratio required during cruise can be found using the method of thrust matching. Recall that, in straight level flight:

$$\left(\frac{T}{W}\right)_{cruise} = \frac{1}{\left(\frac{L}{D}\right)_{cruise}} \tag{3.2}$$

Thus, it is possible to find the power-to-weight ratio required during cruise using our estimation of lift-to-drag ratio from the initial sizing results.

Propeller-driven aircraft optimize range by flying at their maximum lift-to-drag ratio, found to be 13.1 in the previous chapter. Thus, we find that:

$$\left(\frac{T}{W}\right)_{cruise} \approx 0.0763 \frac{\text{lbf}}{\text{lb}}$$

Ratioing this result down to take-off weight and converting it to power-to-weight ratio yields:

$$\left(\frac{P}{W}\right)_{TO} \approx 0.072 \frac{\text{hp}}{\text{lb}}$$

As stated in Raymer, we must pick the biggest of the two values calculated. Thus, a preliminary value for power-to-weight ratio is selected:

$$\left(\frac{P}{W}\right)_{TO} = 0.12 \frac{\text{hp}}{\text{lb}}$$

3.4 Wing Loading Selection

With a selected value of power loading, wing loading is calculated under many constraining conditions. These constraints, along with their formulas, are presented below, and were calculated in an Excel spreadsheet put together by this author. Note that the subscripts on the wing loading denote the constraint, not the flight condition. This is an important distinction, and this convention is followed exclusively in this subsection. Also, calculations are shown for 5000ft. A summary table is provided in the end of the section.

3.4.1 Stall Speed

The stall speed is constrained by the following relationship:

$$\frac{W}{S} = 0.5\rho {V_{stall}}^2 C_{L_{max}} \qquad 3.3$$

Though there are no explicit requirements for stall speed, a typical value of 61kts is assumed, with the idea of possibly ignoring this requirement if it is too much of an outlier later. Computing these for the assumed value of 2.4 for maximum lift coefficient at 5000ft yields:

$$\left(\frac{W}{S}\right)_{stall} \approx 19.5 \frac{\text{lb}}{\text{ft}^2}$$

3.4.2 Takeoff Distance

A FAR compliant takeoff distance requirement for a propeller-driven aircraft is constrained by the following relationship:

$$\left(\frac{W}{S}\right)_{TO} = (TOP)\sigma C_{L_{TO}}\left(\frac{hp}{W}\right) \qquad 3.4$$

Where TOP is the FAR takeoff parameter, whose value is determined to be 145.6 from Roskam[4] and is dependent on the TO distance. Thus, the wing loading at take-off, with a density ratio σ for 5000ft, is calculated to be:

$$\left(\frac{W}{S}\right)_{TO} \approx 22.5\frac{\text{lb}}{\text{ft}^2}$$

Note that the coefficient of lift value used here is not the assumed 2.4. A reasonable assumption is that, during takeoff, the aircraft's speed is $1.1V_{stall}$ to allow for things like gusts of wind. Thus, the coefficient of lift at take-off is $C_{L,max}/1.21$.

3.4.3 Landing Distance

From Raymer[3], the constraining relationship for landing distance is given by:

$$S_{LDG} = 80\left(\frac{W}{S}\right)_{LDG}\left(\frac{1}{\sigma C_{L_{max}}}\right) + S_a \qquad 3.5$$

Where S_a accounts for an obstacle-clearance distance, set to 450ft for STOL type aircraft with a steep glideslope. From this relationship, the calculated wing loading is divided by 0.95 to account for the estimate that $W_{LDG} = 0.95W_{TO}$. Thus, the wing loading for the landing distance constraint at 5000ft is calculated to be:

$$\left(\frac{W}{S}\right)_{LDG} \approx 21.4\frac{\text{lb}}{\text{ft}^2}$$

3.4.4 Cruise and Loiter

To optimize range (cruise) and loiter, respectively, a propeller-driven aircraft's wing loading is restricted by the following constraints:

Cruise
$$\left(\frac{W}{S}\right)_{cruise} = q\sqrt{\pi A e C_{D_0}} \qquad 3.6$$

Loiter
$$\left(\frac{W}{S}\right)_{loiter} = q\sqrt{3\pi A e C_{D_0}} \qquad 3.7$$

Where A is the previously assumed aspect ratio of 10, e is Oswald's Efficiency, assumed to be 0.8, and C_{D0} is the parasite drag coefficient, assumed to be 0.02. Thus, at 5000ft, these values are calculated to be:

$$\left(\frac{W}{S}\right)_{cruise} \approx 94.1 \frac{\text{lb}}{\text{ft}^2}$$

$$\left(\frac{W}{S}\right)_{loiter} \approx 108.2 \frac{\text{lb}}{\text{ft}^2}$$

These values are clearly quite high. They are not used for sizing but just to gather more information about the aircraft, for it might be useful to know what wing loading the aircraft wants for cruise and loiter. Also, the values from Eq. 3.6 and Eq. 3.7 were divided by 0.85 to account for the estimate that $W_{cruise/loiter} = 0.85W_{TO}$. Also, velocity during loiter was estimated to be three quarters of V_max.

3.4.4 Summary and Selection

A table summarizing the results is shown below:

Table 3-1: Wing Loading Summary

Constraint	Condition	Wing Loading [lb/ft^2]
Stall Speed	Sea-Level	30.2
	5000ft	26.1
Takeoff Distance	Sea-Level	34.8
	5000ft	30.0
Landing Distance	Sea-Level	33.2
	5000ft	28.6
Cruise	20000ft	94.1
Loiter	15000ft	108.2

And, after applying a small fudge factor of 0.95 to account for temperature differences and other unaccounted atmospheric and piloting factors, the final preliminary value is selected to be:

$$\left(\frac{W}{S}\right)_0 = 27.2 \frac{\text{lb}}{\text{ft}^2}$$

The stall speed requirement was ignored to allow for a slightly smaller wing that still meets all other more pressing and explicit requirements. It can be shown that, with this wing loading, the following stall speeds are achieved:

$$V_{stall_{sea}} = 57.8\ kts$$

$$V_{stall_{5000ft}} = 62.3\ kts$$

Chapter 4 – Wing Geometry and Layout

4.1 Reference Area

Dividing the maximum take-off weight, W_o, by the preliminary wing loading value of 27.2 lb/ft^2 yields our value for reference area, S_{ref}:

$$S_{ref} = 804.1\ ft^2$$

Which we will use to determine the basic wing geometry and layout.

4.2 Wing Geometry Selection

To select the wing geometry, this author followed a statistical approach. A summary is presented here.

4.2.1 Sweep

Sweep is determined by an observed trend in maximum Mach number vs. sweep. The maximum Mach number is calculated to be 0.42 (maximum speed at FL250) which lands a very low value of sweep:

$$\Lambda_{L.E.} = 5\ deg$$

4.2.2 Taper Ratio

Taper ratio is determined in a manner similar to sweep. An empirical relationship is observed between sweep and taper ratio. For AirSChooner, following the trend for low sweep, subsonic aircraft lands it on the following moderate taper ratio:

$$\lambda = 0.4$$

4.2.3 Twist

There is no widely used statistical equation or physical-based model for determining the appropriate twist for a wing. CFD, wind tunnel testing, and other more advanced methods can be used to optimize this result but are not done in this report. Not much would be learned with the available resources and time. Therefore, a moderate value of -3 degrees is selected for twist, which should provide good enough stall characteristics.

4.2.4 Dihedral

A few factors affect the need for a dihedral, which influences roll stability.

Given the sizing and geometry selection above, the wing will be subsonic with low sweep, calling for some dihedral. However, as will be explained in the configuration downselect, a high wing is a natural choice for this design. High wings naturally create a dihedral effect.

Because of this, this author has decided to not include any dihedral angle. Main considerations are the already stable high-wing configuration, as well as ease of build and manufacturing.

4.2.5 Geometry and Layout

Finally, a table that summarizes the wing geometry, as well as a planform layout of the reference wing, is found below:

Table 4-1: Wing Geometry Summary

S_{ref}	804.1 ft^2
AR	10
$\Lambda_{L.E.}$	5 deg
b	89.7 ft
λ	0.4
C_{root}	12.8 ft
C_{tip}	5.1 ft

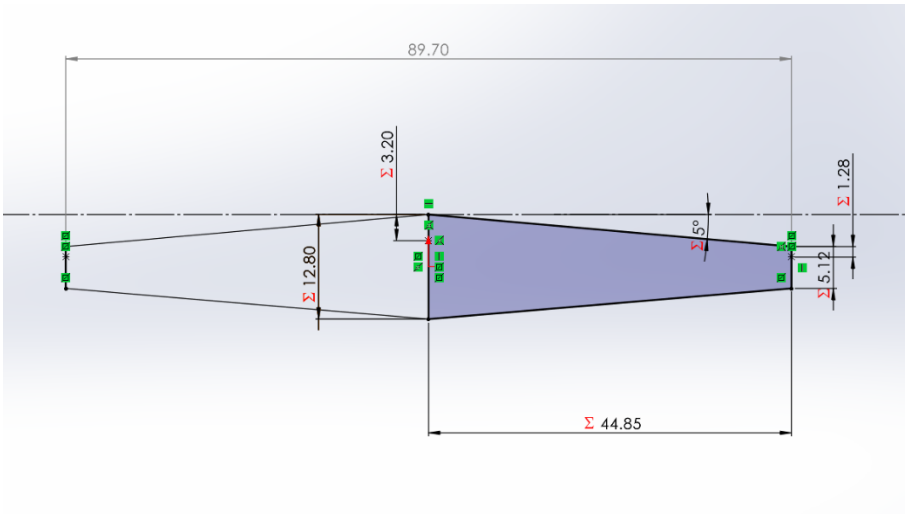

Figure 4.1: Wing Planform Layout (quarter-chord measurements shown)

4.3 Wing Cross-Section

To select an airfoil for the aircraft, a group of roughly twenty airfoils were filtered until four good competitors remained. These finalists are then analyzed, and a reasonable selection is made, as presented below.

For the purposes of this aircraft and mission, a few figures of merit were taken into consideration. A high lift airfoil is needed due to the strong constraints in take-off and landing field lengths. Also, this airfoil is to have gentle stall characteristics, especially considering the tricky nature of water landings. This is also a generally good thing to look for in an airfoil. Other considerations include lift-to-drag ratio, flapped polars, and thickness-to-chord ratio.

4.3.1 Design Lift Coefficient and Airfoil Options

From a larger pool of airfoils, the following were considered finalists for the design:

Table 4-2: Airfoil Finalists Summary

Airfoil	Camber	t/c	Max L/D	Cl_{max}	Cd_{min}
NACA 23012	2%	12%	151.9	1.91	0.005
NACA 3415	3%	15%	157.4	1.97	0.005
Clark Y	3%	12%	174.0	1.94	0.005
Eppler E423	9%	12%	248.6	2.16	0.006

Both NACA 3415 and Clark Y are good examples of "standard" airfoils and are a "safer" bet. The 6-digit series NACA 23012 could provide better stall characteristics due to its better boundary layer control. The Eppler E423 is a very highly cambered airfoil with decent stall and drag characteristics, so was analyzed with the others.

A first order estimate of the design lift coefficient can be found with the following relationship:

$$C_l = \left(\frac{W}{S}\right)\frac{1}{q} \qquad 4.1$$

Assuming cruise flight at FL200, the equation yields:

$$C_l \approx 0.3$$

A reasonable value. A good rule of thumb approximation for 6-digit NACA airfoils given in Raymer[3] is that their camber must be at least 5.5 times the design lift coefficient. This implies a roughly 1.8% camber for this design, hence the choice for the NACA 23012.

4.3.2 Drag Polars

Below are polars for the airfoils mentioned above:

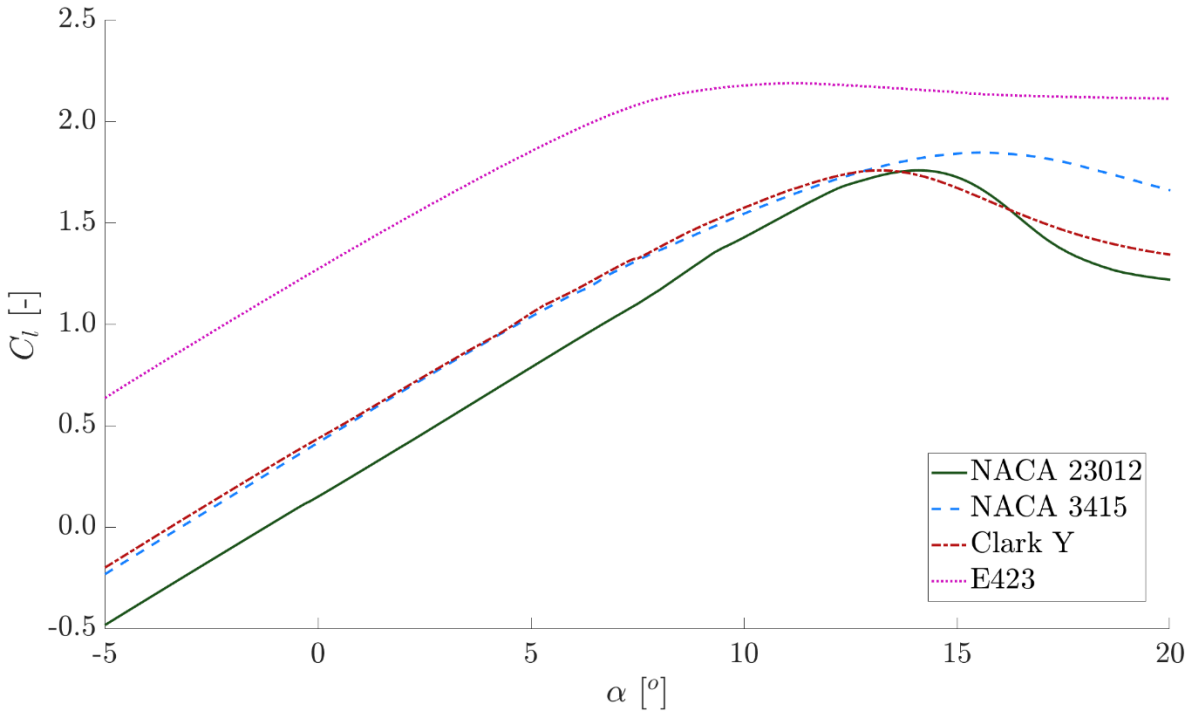

Figure 4.2: Cl vs. Alpha Airfoils

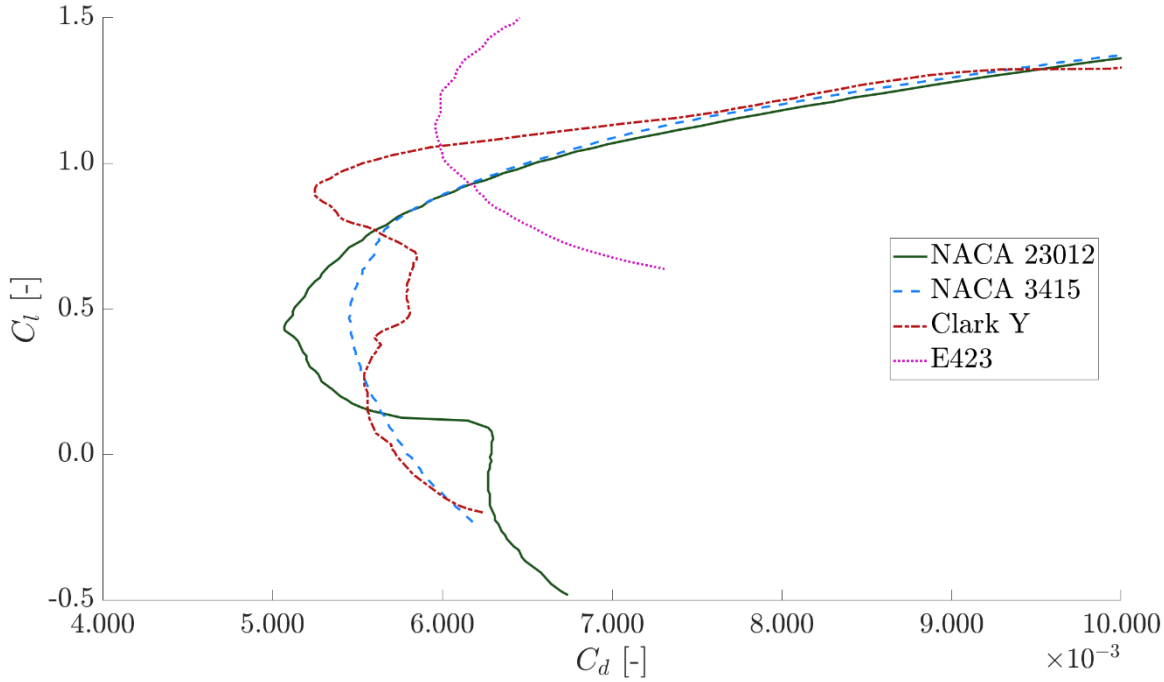

Figure 4.3: Cl vs. Cd Airfoils

These plots were obtained by running Xfoil[5] at a Reynold's number of 10^7 at Mach 0.4, which are representative of the operating range of the aircraft.

The drag bucket above is not characteristic of such a high Reynold's number. Particularly, the Clark Y appears to have "bumps" at moderate coefficients of lift, which is not expected. There was an attempt to remedy this by refining and increasing the number of panels, but that was to no avail. These disparities, though important to note, don't affect the choice of airfoil. The reasons the airfoil was chosen – see below – remain true and can still be seen with the plots above.

4.3.3 Airfoil Selection

After analyzing the polars and considering the different factors for the mission, this author decided to proceed with the NACA 3415.

Its favorable Cl v. Alpha curve, paired with a satisfactory lift-to-drag ratio while maintaining a relatively lower drag coefficient, drove this decision. The higher thickness-to-chord ratio will also help with configuration layout, reduce wing area, and other benefits.

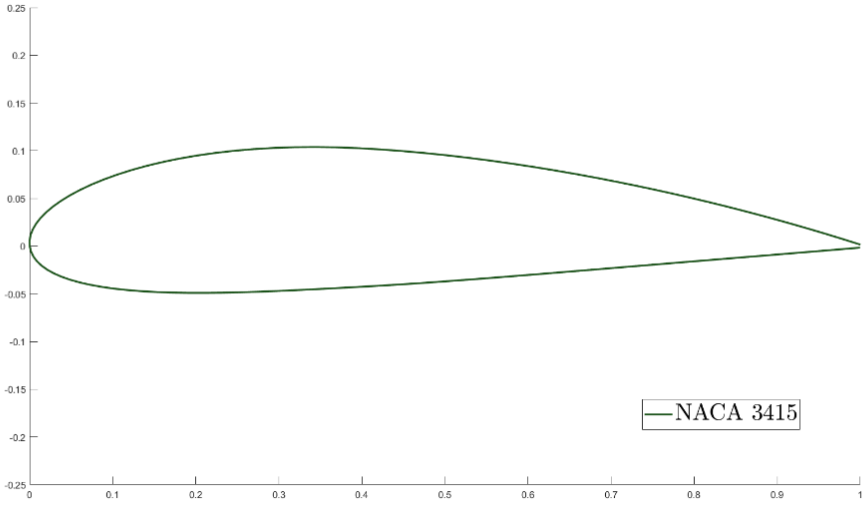

Figure 4.4: NACA 3415 Airfoil

4.4 Wing Layout

With the geometry and cross-section established, a preliminary reference wing can be laid out and is shown below:

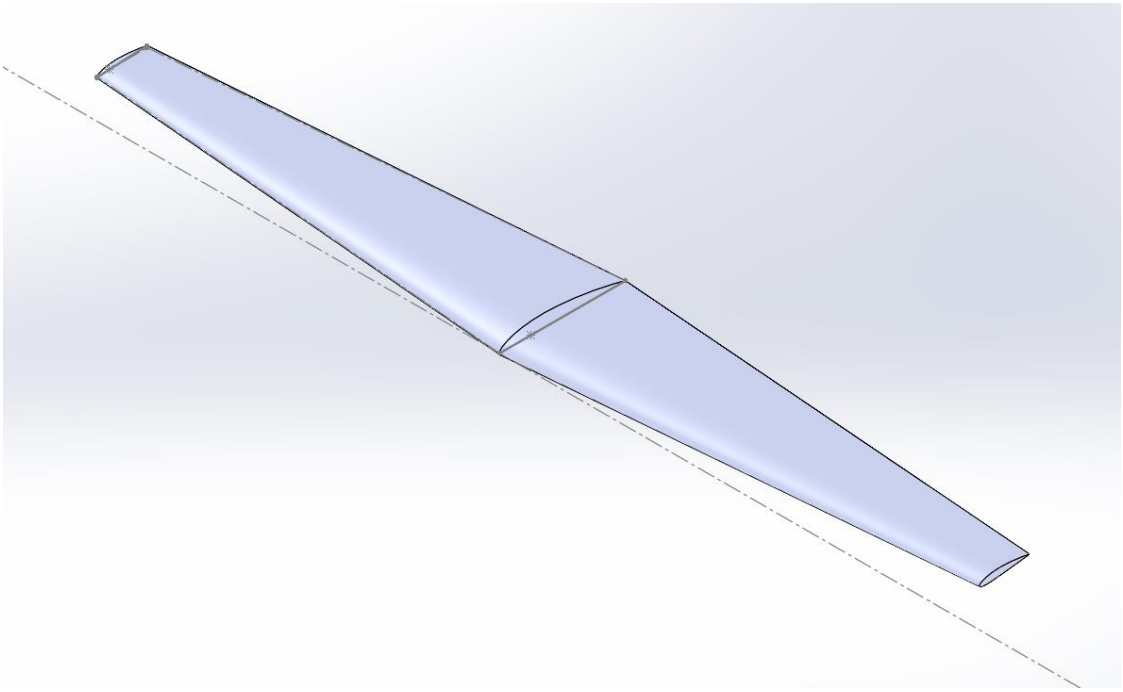

Figure 4.5: Wing Layout Isometric View

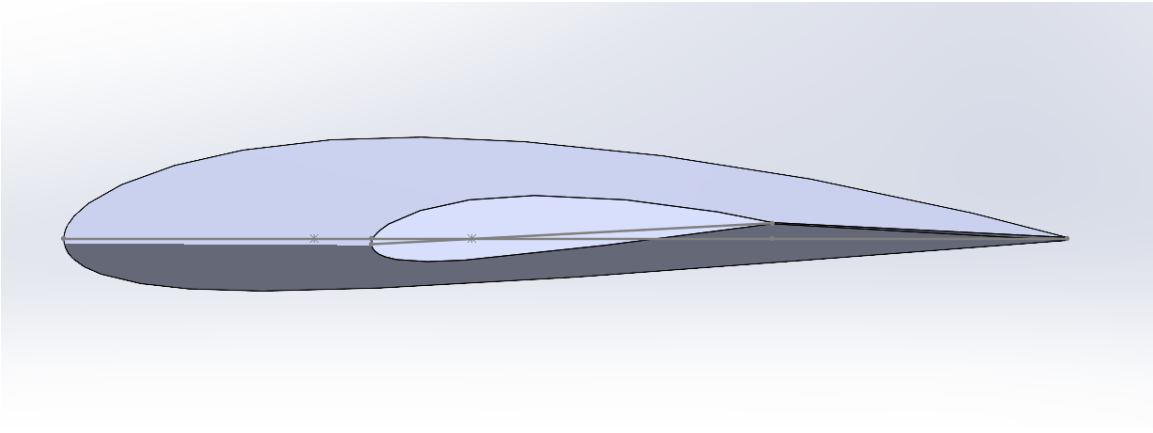

Figure 4.6: Wing Layout Side View (visible twist)

Chapter 5 – Configuration Downselect and Preliminary Geometry Layout

5.1 Configuration Downselect

To select a configuration, a downselect was made for each component based on a few figures of merit (FoM). These FoMs are written out and justified below for each component, and tables are presented.

5.1.1 Aircraft Configuration

A flying boat's configuration is highly constrained by a few factors. The need for a hull on the bottom of the fuselage makes it a challenge to attempt unusual configurations such as flying wings or biplanes. Additionally, some factors constrain the configuration to a small design space. Propeller clearance, water landings, and splash protection are some examples. Still, some options were considered, and a downselect is shown below:

Table 5-1: Aircraft Configuration Downselect

Figures of Merit	Score Factor	Conventional	Biplane	Flying Wing
Hull Placement	0.4	0	-1	-1
Wetted Area	0.3	0	0	1
Stability & Control	0.2	0	0	-1
Complexity	0.1	0	-1	-1
	Total Score	**0**	**-0.5**	**-0.4**

A conventional configuration is a good choice for this mission. Hull placement is convenient in the bottom of the fuselage. Though the wetted area is already increased because of a hull, the complexity and engineering challenges of a flying wing are not worth the marginal benefit in efficiency and reduced surface area.

5.1.2 Wing Placement

Three options were considered: high, mid, and low wing placements. The FoMs, as well as their assigned weights, scores, and final selection, are shown below:

Table 5-2: Wing Placement Downselect

Figures of Merit	Score Factor	Mid-Wing	High-Wing	Low-Wing
Cargo Access	0.3	0	1	-1
Structure	0.3	0	1	1
Stability	0.2	0	1	-1
Water Clearance	0.2	0	1	0
	Total Score	**0**	**1**	**-0.2**

The first FoM considered was cargo access. High wing configurations are generally chosen for cargo purposes, allowing for the rear cargo bay to be easily accessed close to the ground. In the case of a mixed cargo-passenger aircraft, as is the case here, this configuration is still favorable due to the lower height of the fuselage, making cargo doors more accessible.

With regards to structural configurations, mid wings have the issue of the need for a carry-through structure that goes through the fuselage. For this aircraft, that would be right where the passengers are located. This is unfavorable for this mission.

Stability is affected mainly when it comes to roll (or longitudinal) stability. High wings have a natural dihedral effect, as was briefly mentioned in the last chapter. Mid and low wings, on the other hand, have less natural stability. In fact, the latter is naturally less stable in roll.

Finally, water clearance was considered. High wings provide the best clearance from the water so that propellers can be clear of any splash during hard water landings.

5.1.3 Tail Configuration

Three options were considered: conventional, cruciform, and T-tails. A downselect is shown below:

Table 5-3: Tail Downselect

Figures of Merit	Score Factor	Conventional	T-tail	Cruciform
Spin/Stall Recovery	0.4	0	-1	0
Weight	0.4	0	-1	-1
Complexity	0.2	0	0	0
	Total Score	**0**	**-0.8**	**-0.4**

A conventional tail is a good option for this design. T-tails have had some incidents with poor spin recovery. With proper placement, considering the blanketing of the rudder with turbulent wake due to separation on stall, conventional tails can provide appropriate stall recovery characteristics.

Furthermore, t-tails and cruciform tails might suffer a weight penalty. While the top (t-tail) or the middle (cruciform) of the vertical stabilizer would usually only contain ribs, spars, and stringers, the presence of a horizontal stabilizer calls for additional structure, increasing weight. In conventional tails, the placement of the horizontal stabilizer in the fuselage, where robust structure is already present, counteracts this penalty.

5.1.4 Landing Gear Configuration

Three options were considered when it comes to the gear configuration: tricycle, tail-dragger, and bicycle. A downselect is shown below:

Table 5-4: Landing Gear Downselect

Figures of Merit	Score Factor	Tricycle	Tail-dragger	Bicycle
Stability	0.4	0	-1	0
Weight	0.3	0	1	-1
Ground Handling	0.3	0	-1	0
	Total Score	**0**	**-0.4**	**-0.3**

Tricycle gears are a good choice for this design. They are not as light as tail-draggers. In this design, particularly, the gears are to be integrated into the hull, which will add weight and complexity since the hull needs to be sealed and the gears must be retractable.

However, these penalties are present in any configuration for this design. The stability of a tricycle gear with proper placement, especially in contrast to tail-draggers, in addition to its ease of handling on the ground, make it a good choice.

5.2 Main Cabin Layout

To better determine an optimal length of the fuselage, a 2D layout of the cabin was made. This author assumes that the cargo configuration will take significantly less space than the passenger configuration. In other words, cargo can be packed very tightly, but passengers require seats, lavatories, etc. Thus, only the passenger compartment was laid out.

The table below summarizes the values used for seat pitch, width, aisle width, and lavatory area:

Table 5-5: Passenger Cabin Layout Values[3]

Seat Pitch	30in
Seat Width	16in
Aisle Width	15in
Lavatory Area	40inx40in

Furthermore, [4] suggests a rear fuselage length to diameter ratio of 3. The diameter was loosely estimated to be 90in, giving an aft-fuselage length of 270in. The layout, including seats, lavatory, forward cockpit, and aft fuselage, is shown below:

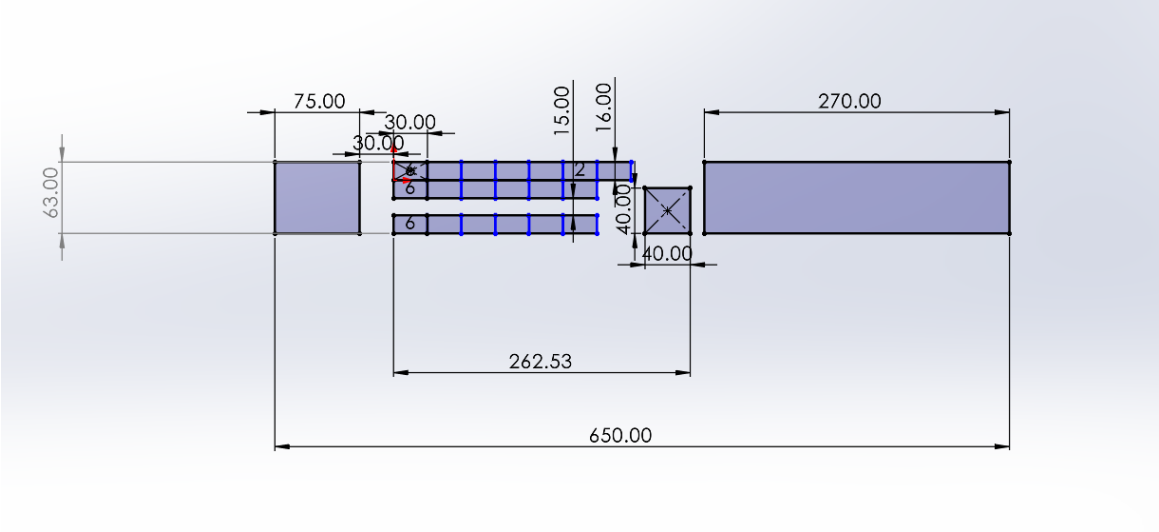

Figure 5.1: Fuselage Cabin Layout

The fuselage length includes the nose portion forward of the cockpit, so would be slightly over the determined 650in. Fuselage length is discussed in-depth below.

5.3 Fuselage Geometry

5.3.1 Beam

The beam of the fuselage can be determined visually based on the layout above.

The width of the cabin was estimated to be 63in. Including a 1in clearance on each side to account for thickness of structural elements of the fuselage, the following is a good estimate of the fuselage's beam:

$$\text{Beam} = 65 \text{ in}$$

5.3.2 Length

The cabin length was estimated to be 650in, or about 54.2ft. With a forward nose portion, the total fuselage length would come in some feet more than that.

The result can be checked against Raymer's statistical approach. In Raymer, the following is a statistically determined expression for fuselage length:

$$l_f = 1.05W_0^{0.4} \qquad 5.1$$

With the calculated value of design take-off weight, the following value for fuselage length is yielded:

$$l_f \approx 57.2 \text{ ft}$$

Which is close to the "empirical" method. Therefore, the fuselage length is chosen to be 57.2ft.

5.3.3 Diameter

The diameter, or height, of the fuselage is determined "visually" and double checked with a few rules of thumb. We can assume the largest diameter is at the passenger compartment. With an aisle height of 65in and an additional 35in for the hull and landing gear, a total maximum diameter of 100in is estimated.

This result is aligned with statistical trends. Roskam[4] points to a fuselage fineness ratio around 6-11 for typical flying boats. A 100in diameter yields a fineness ratio of:

$$\frac{l_f}{d_f} \approx 6.9$$

Which is within the typical range. In fact, it is in the lower end of the range, which is beneficial when it comes to base drag considerations.

5.3.4 Step Height

An important aspect of a seaplane's fuselage is the step. The step is a sudden discontinuity in the bottom of the fuselage, and is present to reduce drag from the water, particularly during take-off since it causes the aft fuselage to lift off when the aircraft is hydroplaning. It also allows the aircraft to be able to rotate at take-off.

A value of 0.05-0.08 times the beam is suggested in Gudmundsson[6] for the step height. This yields the following dimension:

$$\text{Step Height} = 4\,in$$

5.3.5 Additional Considerations

There are some additional considerations when it comes to the layout of a flying boat, particularly when it comes to the hull design and wingtip floats. For these, this author referred heavily to Gudmundsson's Appendix C2[6], which is entirely on the design of seaplanes.

The design of an appropriate hull is of interest. A limited number of hulls on seaplanes are flat bottomed, but most converge in a V-shape for improved hydroplaning. Furthermore, additional edges on the ends of the hull are frequently added. These are called splash rails, and prevent the water from splashing upwards, potentially damaging aircraft components, such as the engines.

Float sizing and design will be conducted after a better estimate of the aircraft's center of gravity is available. The length and beam of the floats are constrained by conditions on the so-called metacentric height of the hull. Though no design decisions were made, this author explored their design at this point.

Gudmundsson presents the following expression for the optimal length of a float:

$$L = 0.7809 W_0^{4/9} \left[\frac{K}{nB}\right]^{1/3} \qquad 5.2$$

Where the constant K is simply 1 for the case of a seaplane with wingtip floats. Plotting the float length for a range of beams yields the following trendline:

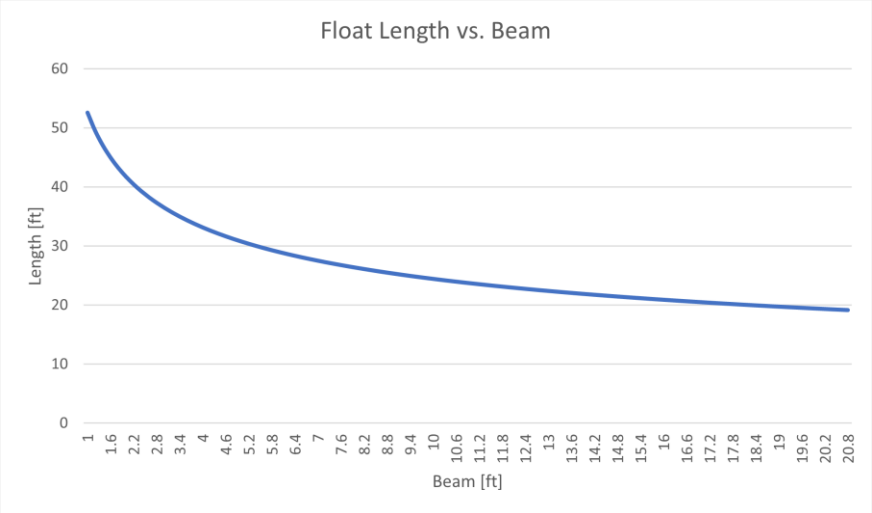

Figure 5.2: Float Length vs. Beam

Which doesn't seem very realistic, but is interesting to keep in mind and will be revisited during layout.

5.4 Powerplant Selection and Placement Considerations

5.4.1 Engine Power

Multiplying the determined power-to-weight ratio by the heaviest design weight yields the value for the required aircraft power output:

$$P = 2625\ hp$$

With a two-engine, wing mounted design, each engine must have the following shaft horsepower rating:

$$P_{shaft} = 1312\ \text{hp}$$

5.4.2 Engine Selection and Size

With a required power, an engine selection can be made.

This author decided to proceed with the Pratt & Whitney PT6A-67F. The engine's power ratings and dimensions are summarized in the table below:

Table 5-6: Pratt & Whitney PT6A-67F Power and Dimensions

Max. Continuous Power	1700 hp
Max. Takeoff Power	1700 hp
Length	75.24 in
Width	18.48 in
Height	18.48 in
Weight	571 lb

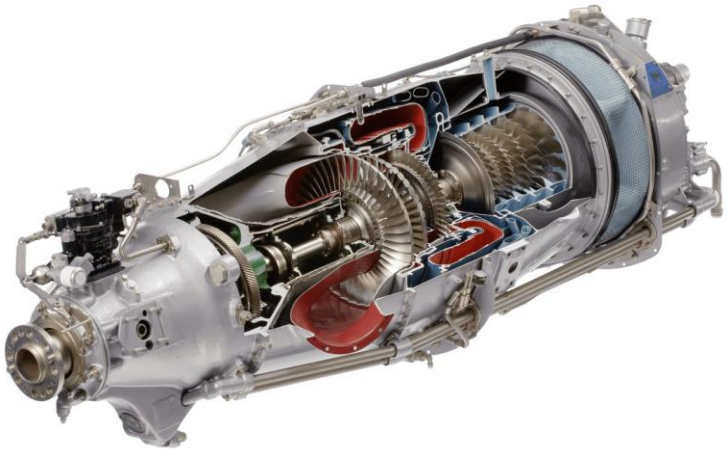

Figure 5.3: PT6A-67F Engine (Credit: Pratt & Whitney)

The engine has more than enough power to sustain the aircraft, exceeding the required shaft horsepower. Furthermore, it has been successfully used in some models of the Air Tractor AT802, a firefighting aircraft with similar characteristics to the one being designed in this report, though with different missions.

An important consideration is engine placement, particularly due to its relatively large length. However, the root and tip chords are, respectively, roughly 154 and 62 inches. It will therefore likely not be a problem to fit a pod-mounted PT6A-67F in the aircraft's wing.

5.5 Propeller Sizing

The propeller's diameter is sized according to the method in [3], where the propeller is sized following a constraint in tip speed and following a statistical method, where the smaller of the two values is chosen.

A propeller's tip speed is given by the following equation:

$$V_{tip} = \sqrt{V_{\text{tip}_{\text{static}}}^2 + V^2} \tag{5.3}$$

Which breaks down the velocity in two components: the propeller's static tip speed, that is, the tip speed if the aircraft was static, and the aircraft's velocity. This describes a helical motion experienced by the propeller tip. The static tip speed is given by:

$$V_{\text{tip}_{\text{static}}} = \pi n D \tag{5.4}$$

Where n is the rotational rate of the engine, and D is the diameter. The following is thus an expression for the diameter of the propellers:

$$D = \frac{\sqrt{V_{\text{tip}}^2 - V^2}}{\pi n} \tag{5.5}$$

Raymer suggests, for metal propellers, that the tip speed should not exceed 950 feet per second. Computing the expression above yields the following value for propeller diameter:

$$D = 9.56 \text{ ft}$$

This value is checked against a statistically determined diameter, given by the following equation:

$$D = K_p \sqrt[4]{P_{\text{shaft}}} \qquad 5.6$$

Where the constant Kp is determined statistically and is different for the cases of 2, 3, and 4+ blades. Computing the expression above for the different constants, the following table summarizes the results:

Table 5-7: Propeller diameter: statistical determination

D (2 blades)	10.23 ft
D (3 blades)	9.63 ft
D (4+ blades)	9.03 ft

For the preliminary layout, the following value for the diameter is then selected:

$$D = 9.03 \text{ ft}$$

5.6 Tail Sizing and Geometry Selection

To size the horizontal and vertical stabilizers, the method of tail volume coefficients was employed. The areas of the horizontal and vertical, respectively, are given by the expressions below:

$$S_{\text{HT}} = \frac{c_{\text{HT}} \bar{C}_W S_W}{L_{\text{HT}}} \qquad 5.7$$

$$S_{\mathrm{VT}} = \frac{c_{\mathrm{VT}} b_W S_W}{L_{\mathrm{VT}}} \qquad 5.8$$

Where c_{HT} and c_{VT} are, respectively, the horizontal and vertical tail volume coefficients, which are approximated to be 0.7 and 0.06 for typical flying boats. Thus, the area of the tails can be determined if their moment arms are known.

A reasonable approximation at this stage is that the moment arm will be approximately 50% of the fuselage length, or 28.6 feet. Thus, the areas are calculated as follows:

$$S_{\mathrm{HT}} = 187.3 \text{ ft}^2$$

$$S_{\mathrm{VT}} = 151.3 \text{ ft}^2$$

The geometry of the tail can be selected and is based on typical values. The aspect ratios of the horizontal and vertical, respectively, are selected as 4 and 1.5. The taper ratios are selected as 0.5 and 0.6. The table below summarizes the geometry of the tail:

Table 5-8: Tail Geometry Summary

Geometry	Horizontal Tail	Vertical Tail
S_{ref}	187.3 ft^2	151.3 ft^2
AR	4	1.5
λ	0.5	0.6
C_{root}	9.1 ft	12.6 ft
C_{tip}	4.6 ft	7.5 ft
MAC	7.1 ft	10.3 ft
b	27.4 ft	15.1 ft
$\Lambda_{L.E.}$	9.5 deg	18.4 deg

5.7 Preliminary Layout

With most of the geometry selected and sized, a preliminary layout of the basic geometry of the aircraft can be made. A four-view diagram of the layout, carried out in OpenVSP[7], is shown below:

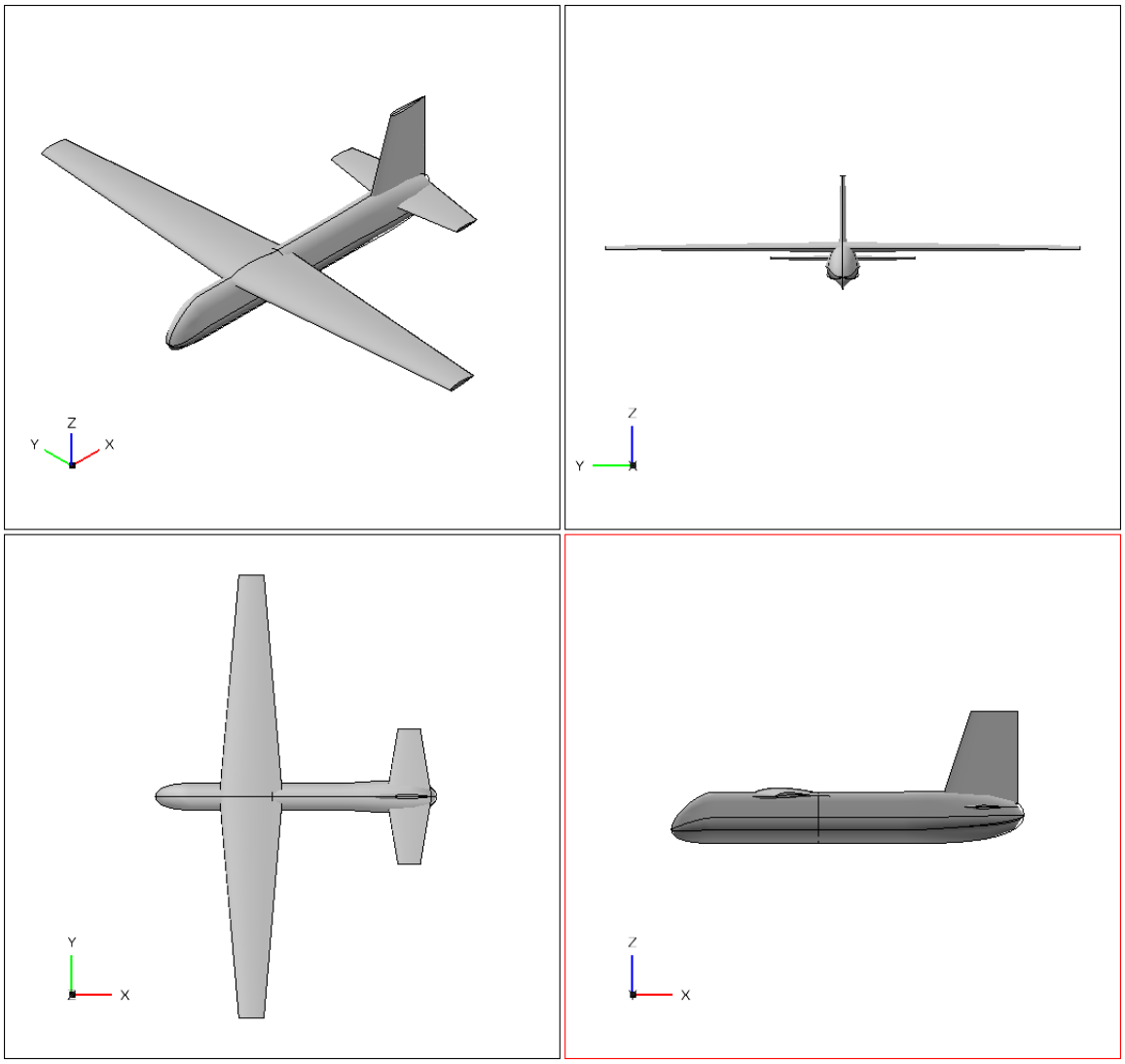

Figure 5.4: First Preliminary Layout Four-View

It is clear that major aspects of the aircraft are missing. This is because many components or characteristics of the aircraft, namely the hull step and landing gears, are heavily dependent on the longitudinal location of the center of gravity. Thus, an estimate of C.G. must be made based on an estimation of component weights, after which the layout can be revisited.

Chapter 6 – CG Estimation and Revised Layout

6.1 Landing Gear Sizing

A preliminary sizing of the landing gears is performed prior to the revised layout.

Raymer provides statistical expressions for the determination of the diameter and width of the wheels as a function of the weight supported by them. It is important to note "wheels" in this case refers to the wheel/brake/tire assembly, not only the metal portion which the tires are attached to.

The width and diameter, respectively, are given by:

$$\text{Width} = 0.7150(W_W)^{0.312} \tag{6.1}$$

$$\text{Diameter} = 1.51(W_W)^{0.349} \tag{6.2}$$

As a good first order approximation, the nose wheels can be estimated to be 60-100%. Thus, the width and diameter are found. Also, it is reasonable to assume that the main wheels will support 90% of the weight of the aircraft. Thus, the dimensions are found to be:

$$\text{Width} = 12.6 \text{ in}$$

$$\text{Diameter} = 37.4 \text{ in}$$

6.2 Powerplant Placement

Three main considerations were taken when placing the two wing-mounted engines.

In the last chapter, the blade diameter was estimated to be around 9 feet. Thus, it is clear that a primary consideration is the clearance of the blades from the fuselage. The minimum clearance is the radius. However, additional space is given for many reason. Blade tip-fuselage interactions, cabin noise, and wing space are just a few considerations.

Secondly, it is important to consider engine-out scenarios. The further the engines are spaced out, the larger the yawing moment produced by the operating engine in case of one engine out situations.

Lastly, [4] suggests a spacing of at least half times the chord between the blades and the wing's leading edge. This author took this rule into consideration when placing the engines.

The figure below shows the preliminary placement of the engines:

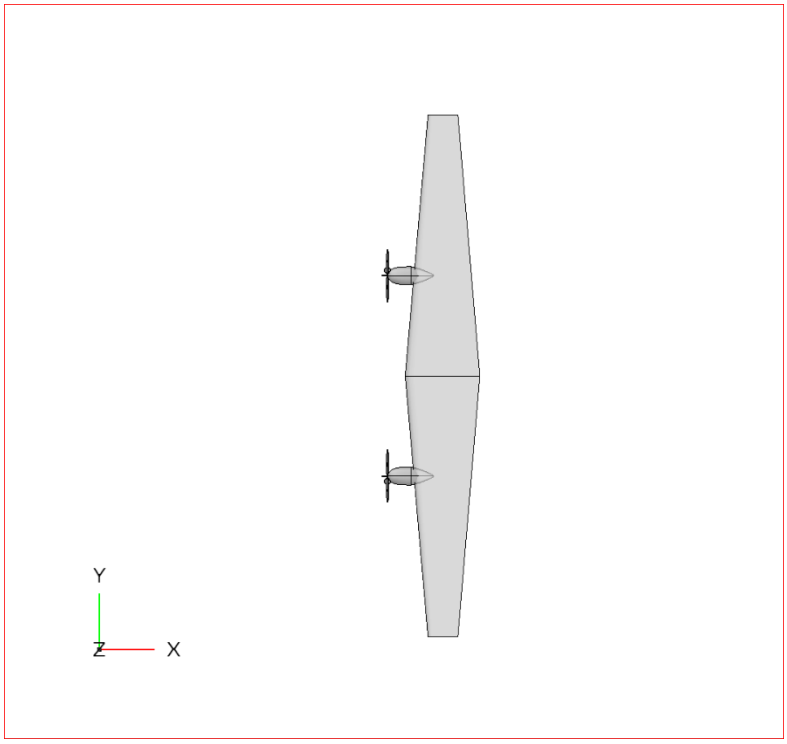

Figure 6.1: Powerplant Placement

6.3 Fuel System Sizing and Placement

Another important system to consider that influences CG is the location of the fuel tanks.

Given the large wing area due to performance requirements and a moderate thickness-to-chord ratio of the chosen airfoil, using internal tanks, specifically integral tanks, also known as wet wings, is a reasonable choice.

To calculate the required fuel weight, the fuel weight fraction obtained during preliminary sizing for each mission is multiplied by the design take-off weight of each mission. Computing this yields the following maximum fuel weight:

$$W_{\text{fuel}} = 2231 \text{ lb} \qquad 6.3$$

Which is the flown during passenger missions. To find the volume required, the value is divided by the density of JET-A at 59 °F[3]. The required tank volume is thus:

$$V_{\text{fuel}} = 44.5 \text{ ft}^3 \qquad 6.4$$

The tanks are placed conformally in the wing, and their locations are shown in the figure below:

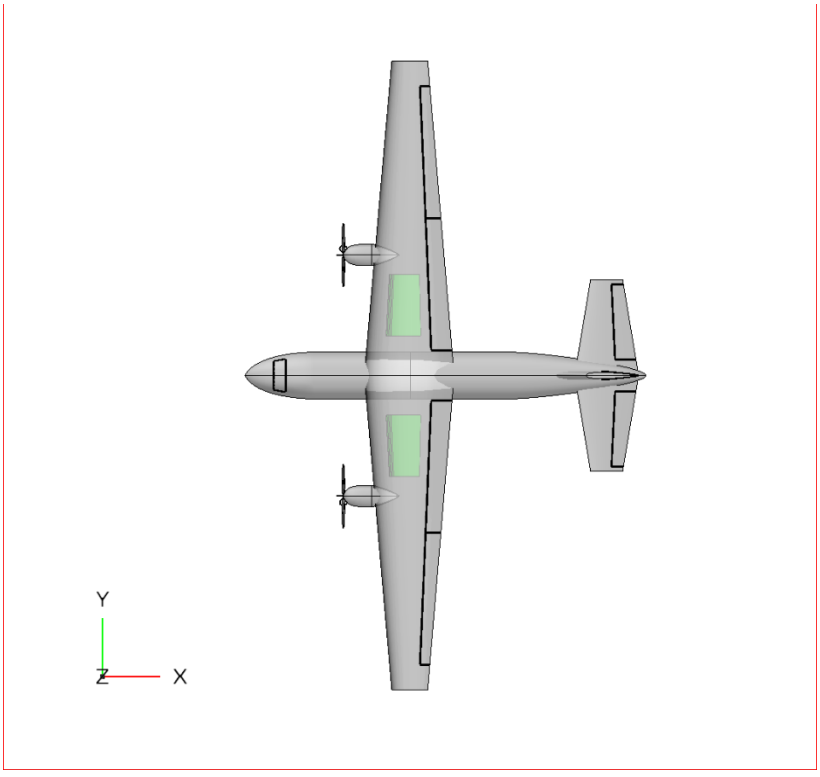

Figure 6.2: Fuel Tank Locations

6.4 CG Estimation

6.4.1 Overview

The center of gravity is estimated in two ways: first, a rough method is used to estimate the empty weight CG. This is referred to as a class I estimate. Then, a more involved method is used to determine the center of gravity location more precisely. This method involves statistical equations for subsystems of the aircraft as functions of a good number of values. This is referred to as a class II estimate.

.6.4.2 Class I Estimate: Empty Weight Buildup

First, the weights of major aircraft components are estimated based on a rough statistical model[3]. In this model, constants are multiplied by reference parameters specific to the component to find the weight. For instance, the wing weight has its exposed planform area as its reference parameter, which is multiplied by a constant to find the weight.

These constants depend on the type of aircraft, and are divided between fighters, transport & bomber, and general aviation. This author chose constant values somewhere between the transport& bomber category and general aviation category. Additionally, a "fudge factor" was applied to the fuselage weight to account for added weight of the hull.

The table below summarizes the weight calculations and the longitudinal location with respect to the datum, taken as the aircraft's nose and found/manipulated in OpenVSP based on the preliminary layout:

Table 6-1: Class I Weights

Component	Weight [lb]	XLoc [ft]
Wing	3566	18.5
Horizontal Tail	498	50.9
Vertical Tail	409	48.9
Fuselage	2041	22.9
Main Gears	1060	23.0
Nose Gear	187	10.0
Installed Engines	1599	14.0
All-else Empty	3281	22.9

The longitudinal locations for the wing, horizontal tail, and vertical tail are taken as 40% of the MAC of the respective surfaces. Given the root's leading-edge location, X_{LE} (which is what is input into the software), the leading-edge sweep, the spanwise location of MAC, and the MAC, it is possible to find the longitudinal location of a fraction of the MAC like so:

$$X_{n\%_{MAC}} = X_{LE} + \bar{Y}\, tan(\Lambda_{LE}) + (\frac{n}{100})MAC \qquad 6.5$$

The fuselage location was taken as 40% of its length. The same was taken for "all-else empty," which accounts for the rest of empty weight, such as avionics and other subsystems. The location of gears was changed around until a satisfactory stability and arrangement was achieved. All calculations were made in an Excel spreadsheet.

Multiplying the weights by the locations to find moments and dividing by total empty weight, the CG is found to be:

$$X_{C.G.} = 22.3 \text{ ft}$$

And the empty weight:

$$W_{\text{empty}} = 12{,}640 \text{ lb}$$

Which is within 12% to what was estimated during the initial sizing iterations, an acceptable result.

6.4.3 Class II Estimate: Statistical Weights

The weight of a few subsystems of the aircraft and other relevant components, such as crew and passengers, seats, etc., are calculated to find a more accurate position of the center of gravity. These weights are found using a statistical approach[3]. The calculations were done using an Excel spreadsheet.

The table below summarizes the results of the class II CG estimation:

Table 6-2: Class II Weights

Component	Weight [lb]	XLoc [ft]
Wing	3566	22.5
Horizontal	498	50.9
Vertical	409	48.9
Fuselage	2041	22.9
Main Gears	1060	32.2
Nose Gear	187	7.5
Installed Engine	1792	14.0
Fuel System	173	18.5
Flight Controls	812	30.0
Hydraulics	198	37.5
Avionics	1082	3.0
Electrical	478	35.0
AC and Anti-Ice	1161	35.5
Furnishings	1143	21.0
Fuel	2231	23.4
Passengers + Crew	4620	22.4
Pilots + Seats	484	7.0
TOTAL WEIGHT [lb]	21,935.73	

Thus, a more accurate estimation of the CG location is found to be:

$$X_{C.G.} = 23.4\ ft$$

It is worth to note a few things. Furnishing includes seats, insulation, trim panels, lavatories, galleys, lighting, wiring, among other things[4]. Also, the longitudinal location of components was determined by comparison to other aircraft and where the subsystem in these aircraft is located. Lastly, note the change in the location of the landing gear and wing from the class I estimate. This will be reflected in the revised layout and was done for stability reasons.

6.5 Revised Geometry

6.5.1 Hull Beam and Step

During the preliminary geometry layout, this author noted that the cabin seemed narrow. This was confirmed when fitting a 95th percentile human being in the layout software utilized. Looking at similar aircraft in Roskam[4], particularly ones with a 2+1 seating configuration, it was found that their widths are in the range of 75-90 inches. Thus, the new beam was determined to be 80 inches, and the new step height 6.4 inches. Splash rails were also added to the hull. The cross section of the fuselage is shown below:

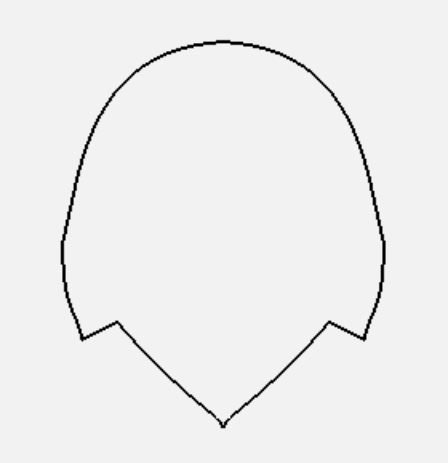

Figure 6.3: Fuselage Cross-Section (main cabin, forward of step)

6.5.2 Wingtip Floats Sizing

Figure 5.1 represents an attempt to size the floats using methods found in literature. However, the results are not in line with what is seen in other aircraft.

This author decided to take a different approach. Instead, the float length for a known aircraft would be determined and scaled based on a non-dimensional parameter. For the choice of this parameter, it seems imperative that it be dependent on weight due to its relationship to buoyancy. Thus, wing loading was selected. The float length is then determined as:

$$L_{\text{AirSChooner}} = \left(\frac{W/S_{\text{AirSChooner}}}{W/S_{\text{Comparison}}}\right) L_{\text{Comparison}} \qquad 6.6$$

The Beriev BE-200 was used as a comparison metric for its availability in Jane's All The World Aircraft[2]. With the method above, the float length is found to be:

$$L_{\text{AirSChooner}} = 6.95 \text{ ft}$$

The beam was modelled after the Beriev's approximate fineness ratio, and was determined to be:

$$\text{B}_{AirSChooner} = 2.30 \; ft$$

The tip floats are mounted under airfoil-shaped pylons and are position along the wing such that the angle between the mid-point of the hulls is approximately 4 degrees for reasonable water stability.

6.5.3 Control Surface Sizing

Lastly, the control surfaces were sized. These are the flaps, ailerons, rudder, and elevator.

All sizing was done according to Raymer's guidelines and by looking at similar aircraft[2,3,4]. It is suggested and verified historically that flaps span from the fuselage-wing intersection to about half the span, while the ailerons extend to roughly 90% of the span. Not much lift is gained in the last 10% of the span due to wingtip vortex effects.

Rudders and elevators extend from the root to either the end of the surface or about 90% of the span. It is worth noting that these control surfaces have higher percent chords to increase the control surface area (given the smaller reference area of the tail compared to the wing).

The table below summarizes the control surface sizing:

Table 6-3: Control Surface Sizing

Control Surface	$C_{surface}/C$
Flaps	0.25
Aileron	0.25
Elevator	0.36
Rudder	0.45

6.6 Revised Layout

Below is the revised layout. Besides a four-view diagram, some figures of interest are presented:

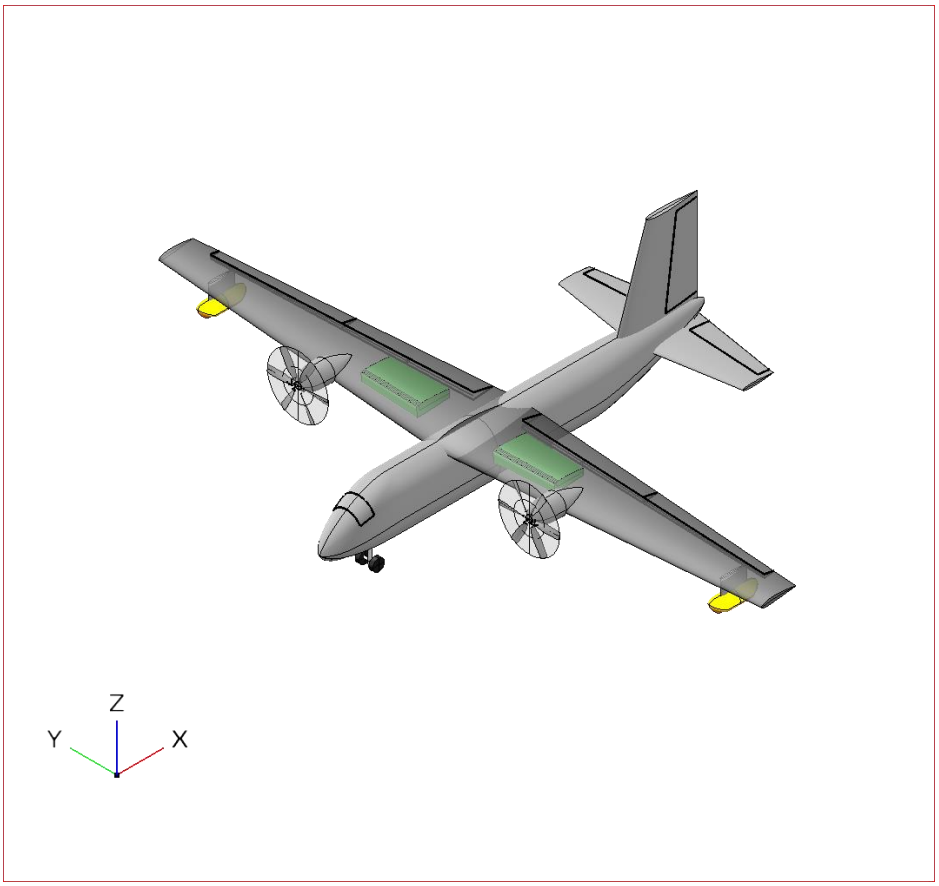

Figure 6.4: Revised Layout: Isometric View

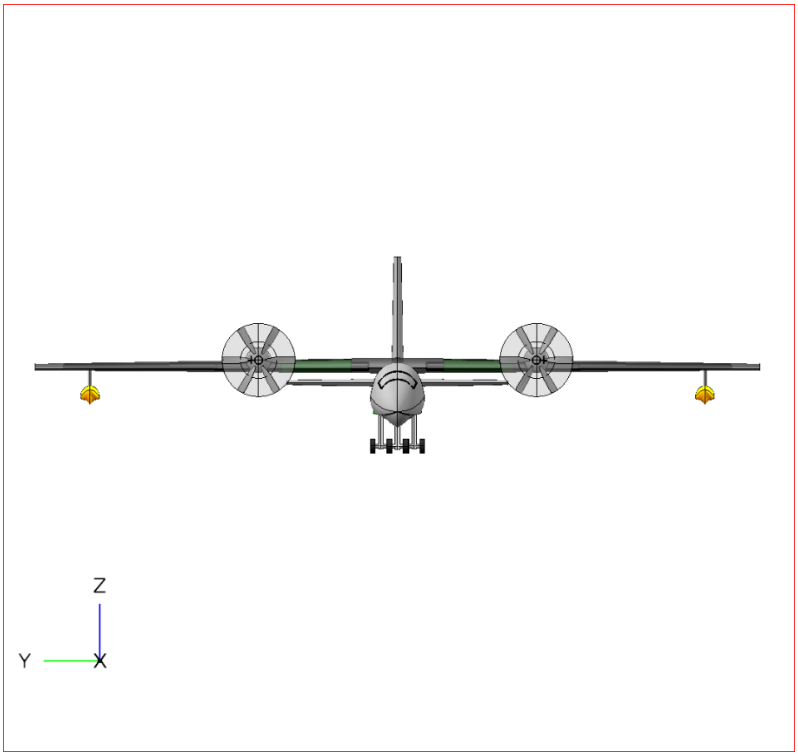

Figure 6.5: Revised Layout: Front View

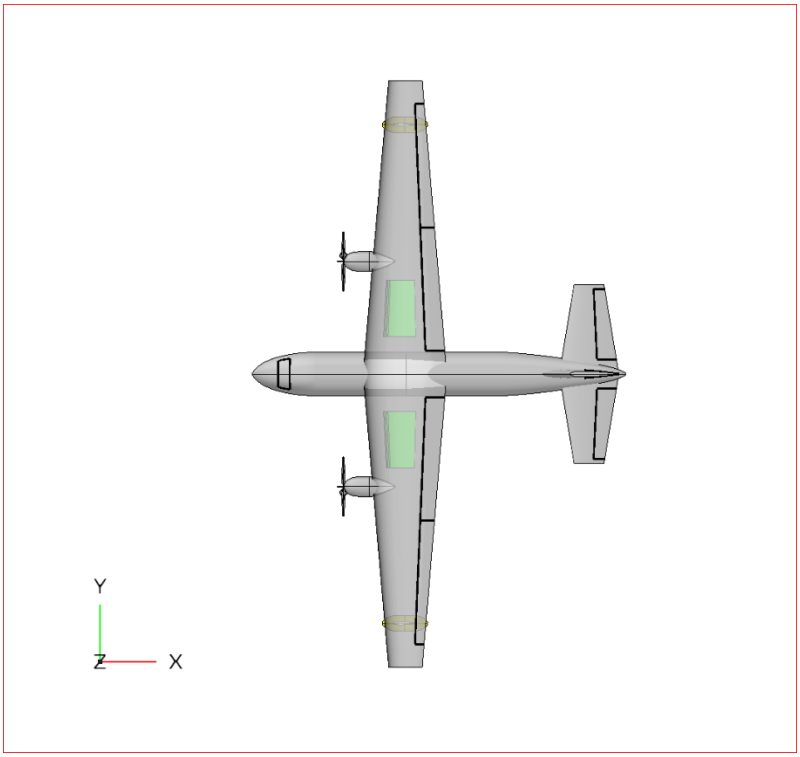

Figure 6.6: Revised Layout: Top View

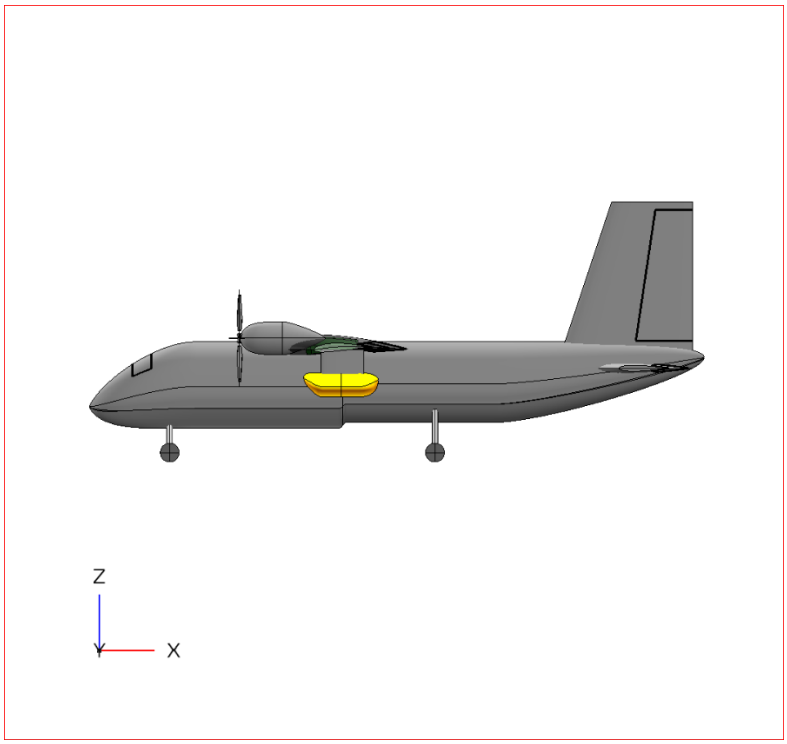

Figure 6.7: Revised Layout: Side View

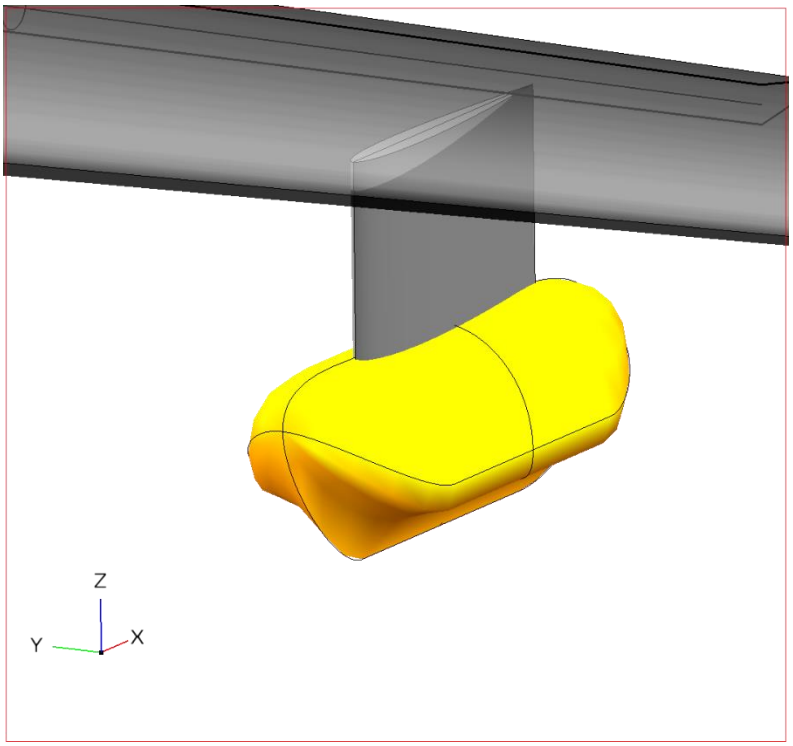

Figure 6.8: Revised Layout: Wingtip Float

6.7 Additional Comments/Observations

6.7.1 Landing Gear Stowage

It is important to ensure that the landing gears can be stowed underneath the passenger compartment. A side view representative of the stowage is shown below:

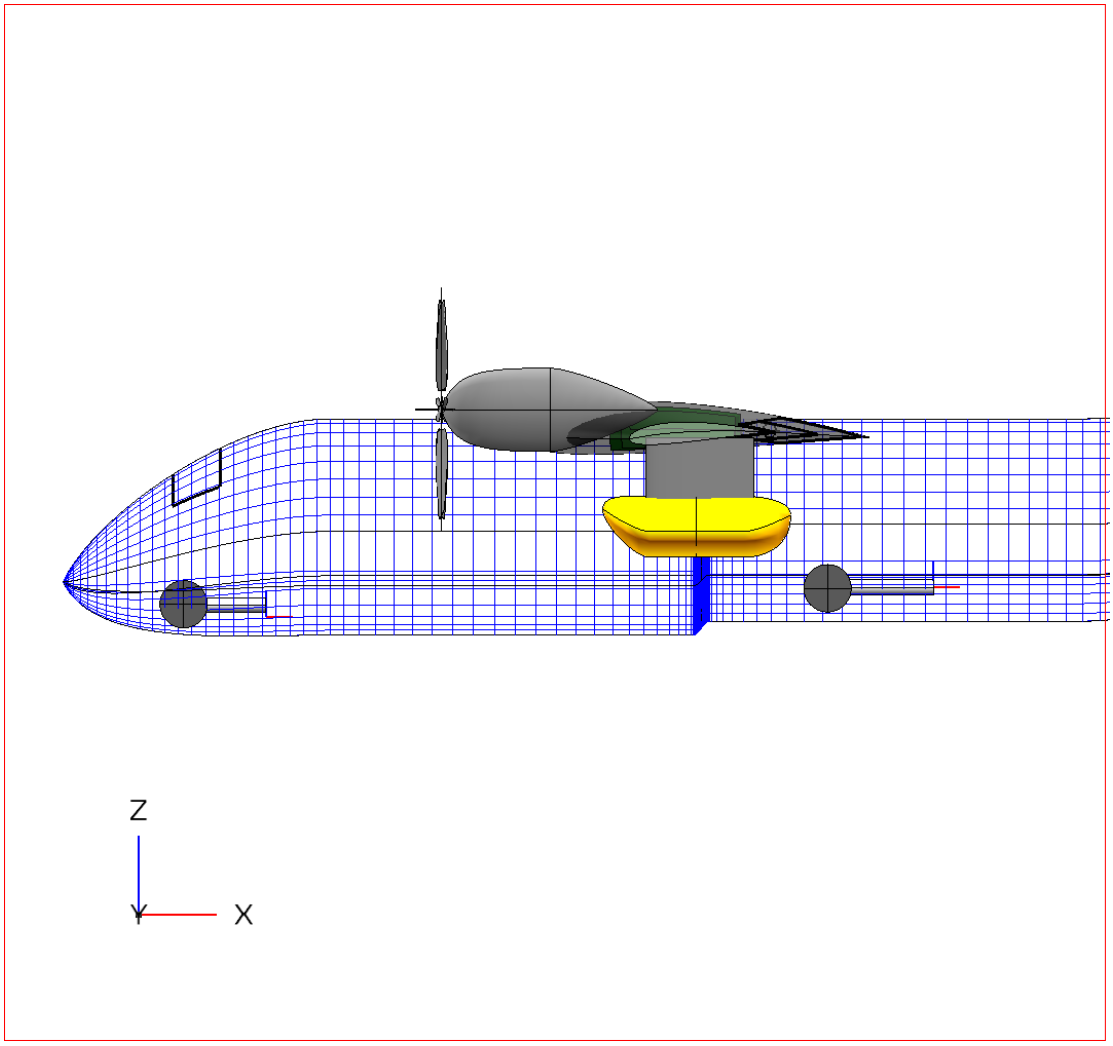

Figure 6.9: Revised Layout: Landing Gear Stowage

Notice that the gears are chosen to be retracted forward, that is, they rotate towards the aft when deployed. This is in case a hydraulic malfunction occurs, in which case the gears naturally drop to the deployed position and are held there due to aerodynamic drag.

6.7.2 Rotation Angle

It is also important to ensure that the aircraft is able to rotate enough for take-off and flare during landing. The rotation angle, from the rear gears to the tail tip, is measured in the software and shown below:

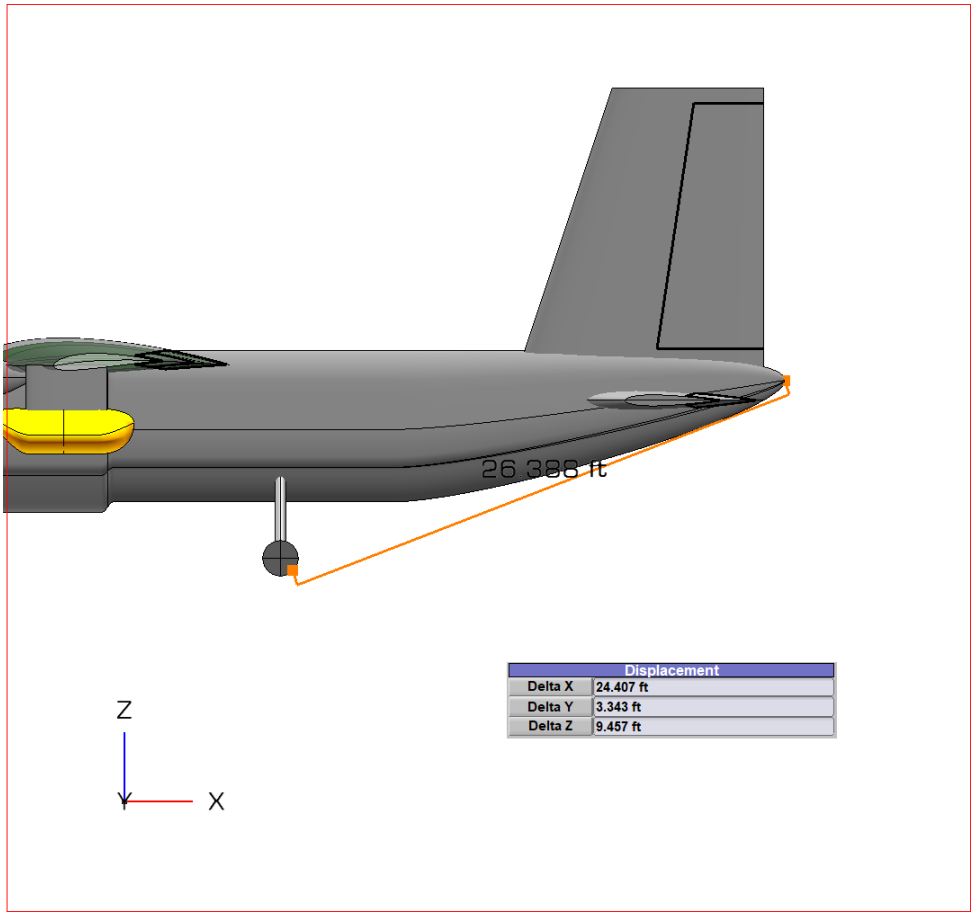

Figure 6.10: Revised Layout: Rotation Angle

The rotation angle is then estimated to be:

$$\alpha_{rot} \approx tan^{-1}\left(\frac{\Delta Z}{\Delta X}\right) \approx 21.2 \text{ deg}$$

Which is higher than the stall angle for the airfoil used and thus high enough to extract all the lift out of the wing before rotation.

6.7.3 Waterline and Propeller Clearance

One important consideration in the vertical location of the propeller is the water clearance. It is important that the propeller stays well clear of the water, especially when the aircraft is in its full weight resting on the water, since that is the situation where the most water is displaced.

Pure water has a density of around 62.4 pounds per cubic feet, such that AirSChooner displaces, in its maximum weight configuration, about 350 cubic feet of water. Within OpenVSP, the height of the waterline can be found by finding a component conformal to the bottom of the hull whose volume is 350 cubic feet. The waterline is then determined to be remarkably close to the nose and is shown in the figure below. Notice also how the tip floats would strike the water before the propellers in case of rolling motion:

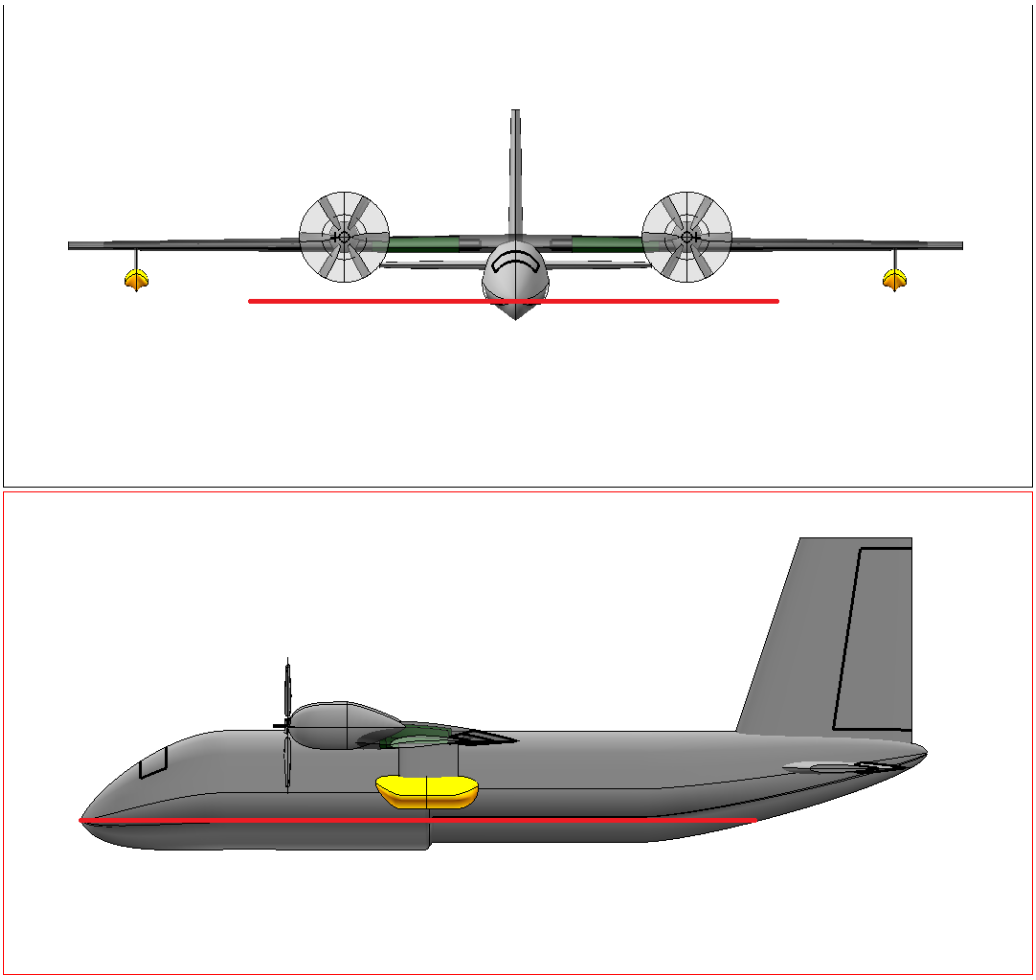

Figure 6.11: Revised Layout: Waterline Clearance

Chapter 7 – Aerodynamics

7.1 Overview

This chapter presents the aerodynamic analysis of the as-drawn aircraft of the previous chapters. The analysis follows the methods in Raymer and Roskam[3,4], and also includes computational analysis with simple panel method codes in OpenVSP[7].

It is worth noting that the operating envelope of this aircraft simplifies the analysis. With a cruising Mach number of approximately 0.4, AirSChooner flies in the lower-mid subsonic range. Therefore, supersonic aerodynamics is not quite relevant to the analysis. However, trends at higher Mach numbers are shown regardless.

7.2 Lift-Curve Slope

The lift curve slope can be estimated with the following equation:

$$C_{L_\alpha} = \frac{2\pi A}{2 + \sqrt{4 + \frac{A^2\beta^2}{\eta^2}\left(1 + \frac{tan^2\,\Lambda_{max,t}}{\beta^2}\right)}}\left(\frac{S_{exposed}}{S_{ref}}\right)(F) \qquad 7.1$$

Where β is the reciprocal of the Prandtl-Glauert compressibility correction factor, given by:

$$\beta = \sqrt{1 - M^2} \qquad 7.2$$

And η is the airfoil efficiency, given by:

$$\eta = \frac{C_{l_\alpha}}{2\pi/\beta} \qquad 7.3$$

And F is the fuselage lift factor, given by:

$$F = 1.07\left(1 + \frac{d}{b}\right)^2 \qquad 7.4$$

If the product of the fuselage lift factor and the ratio of exposed to reference area of the wing is greater than one, that implies that the fuselage creates more lift than the wing it covers, which is unlikely, so the product is set to 0.98.

A plot of the lift-curve slope at a range of Mach numbers is shown below:

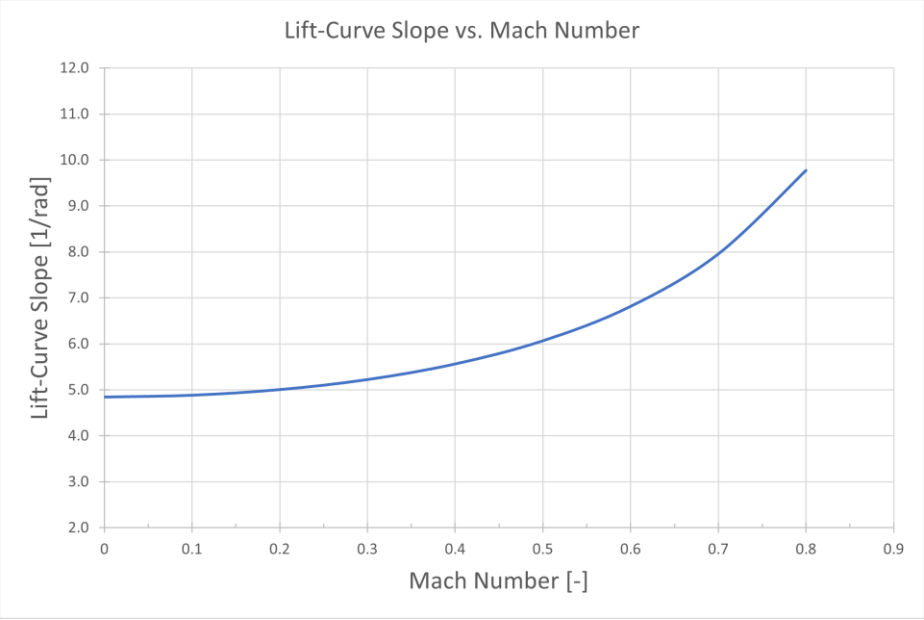

Figure 7.1: C_{L_α} versus Mach number

7.3 $C_{L_{max}}$ estimation

7.3.1 Aspect Ratio

A wing of high aspect ratio is one that obeys the following expression:

$$AR > \frac{3}{(C_1 + 1)(cos\,\Lambda_{L.E.})} \qquad 7.5$$

Where C_1 is a constant that depends on the taper ratio and is found in a figure in Raymer[3]. Computing this for the values in AirSChooner, the expression stands. Thus, aerodynamic calculations for high aspect ratio wings are appropriate.

7.3.2 Clean $C_{L_{max}}$

The maximum clean coefficient of lift can be found as a function of Mach number. It is given by the following expression:

$$C_{L_{max}} = C_{l_{max}} \left(\frac{C_{L_{max}}}{C_{l_{max}}} \right) + \Delta C_{L_{max}} \qquad 7.6$$

In the expression above, $\frac{C_{L_{max}}}{C_{l_{max}}}$ is found in a figure as a function of leading-edge sweep and the leading-edge sharpness parameter, Δy, defined for NACA 4-digit airfoils to be 26 times the thickness-to-chord ratio. $\Delta C_{L_{max}}$ is found in a figure also as a function of sharpness parameter, as well as Mach Number.

The first value, $\frac{C_{L_{max}}}{C_{l_{max}}}$, is found to be 0.88. A table can be formulated for the $\Delta C_{L_{max}}$ values as functions of Mach number:

Table 7-1: $\Delta C_{L_{max}}$ for a range of Mach numbers

Mach Number	$\Delta C_{L_{max}}$
0.2	0
0.3	-0.22
0.4	-0.38
0.5	-0.5
0.6	-0.58

Then, the maximum lift coefficient can be calculated and plotted against Mach number:

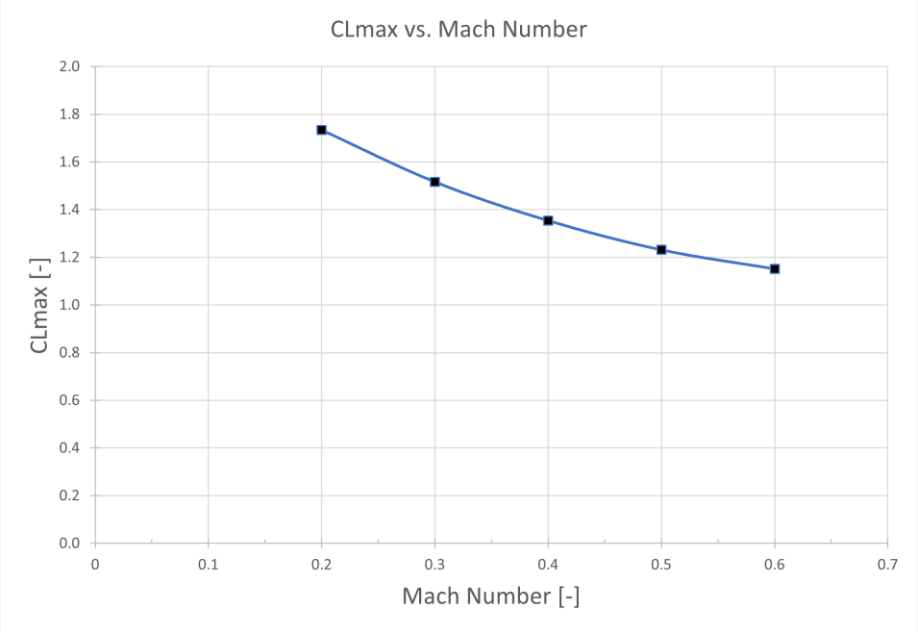

Figure 7.2: $C_{L_{max}}$ versus Mach number

The angle of attack at maximum lift coefficient can be found in a similar manner with the following expression:

$$\alpha_{C_{L_{max}}} = \frac{C_{L_{max}}}{C_{L_\alpha}} + \alpha_{0L} + \Delta\alpha_{C_{L_{max}}} \qquad 7.7$$

Which is plotted against Mach number below:

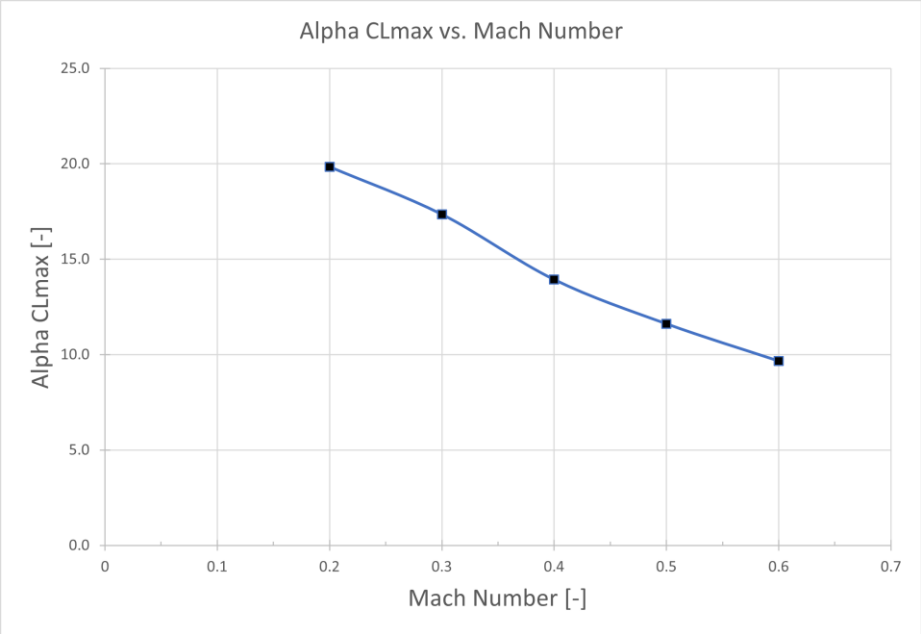

Figure 7.3: $\alpha_{C_{L_{max}}}$ versus Mach number

7.4 High Lift Devices

The gain in coefficient of lift is given by the following expression:

$$\Delta C_{L_{max}} = 0.9 \Delta C_{l_{max}} \left(\frac{S_{\text{flapped}}}{S_{\text{ref}}} \right) cos\, \Lambda_{\text{H.L.}} \qquad 7.8$$

Where $\Delta C_{l_{max}}$ depends on the type of high-lift device used and is found in a table in Raymer[3], S_{flapped} is the flapped area of the wing, and $\cos \Lambda_{\text{H.L.}}$ is the cosine of the angle of the hinge line (in this case, $\Lambda_{\text{H.L.}} = \Lambda_{\text{T.E.}}$) The flapped area of the wing is the entire area of the wing where there is a control surface present. It is not solely the area of the control surface.

The table below summarizes the change in maximum coefficient of lift for each high-lift device type:

Table 7-2: $\Delta C_{L_{max}}$ for different flap types

Flap Type	$\Delta C_{L_{max}}$
Plain and split	0.42
Slotted	0.61
Fowler	0.64
Double slotted	0.79
Triple slotted	0.94

And below is the maximum lift coefficient for various Mach numbers and flap types:

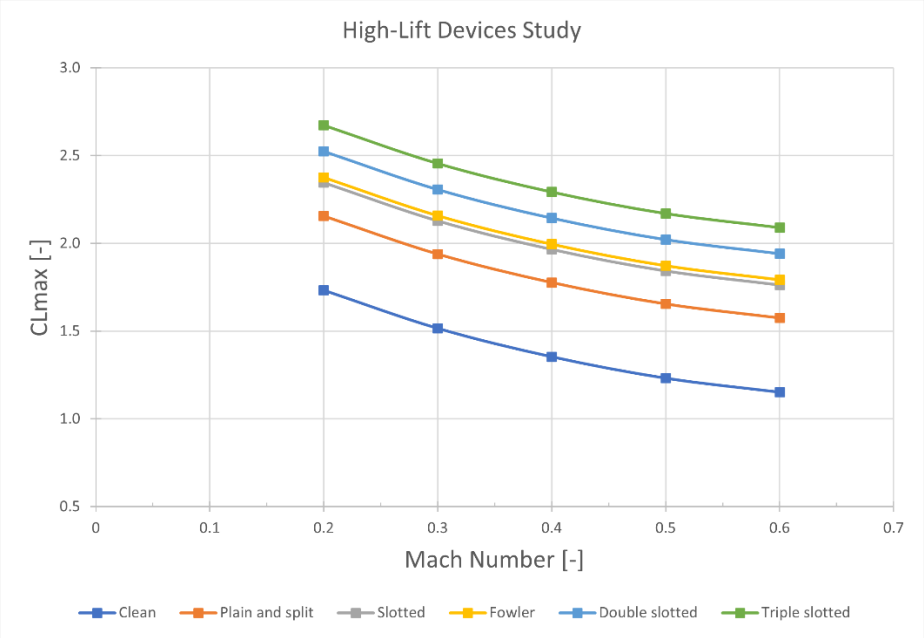

Figure 7.4: $C_{L_{max}}$ versus Mach number for various flap configurations

Considering the added complexity of more intricate flap systems and the weight associated with them, slotted flaps are a good option for this design. Their low complexity and high maximum coefficient of lift at moderate Mach numbers make them ideal for the STOL nature of this aircraft.

7.5 Parasite Drag Buildup

A drag buildup can be done internally to the layout software. Each component has its wetted area calculated, and a form factor correction is calculated. The software gives the user the choice between various form factor corrections equations, most notably Hoerner and Torenbeek. This author computed parasite drag with both methods, and the difference was negligible. The figures below are computed with Hoerner's methods.

Two pie charts representing the parasitic drag buildup in both clean and dirty configurations are shown:

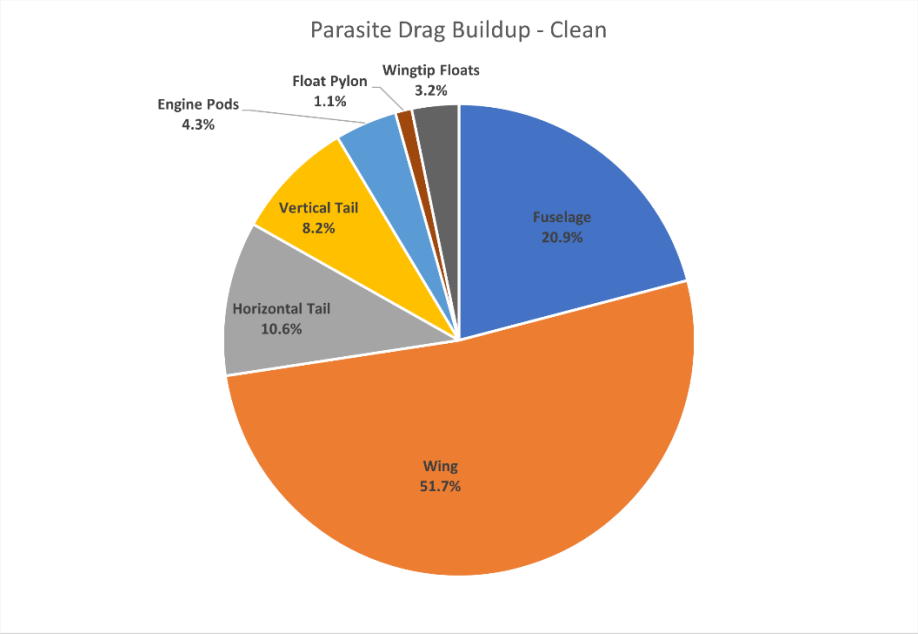

Figure 7.5: Parasite Drag Buildup (Clean)

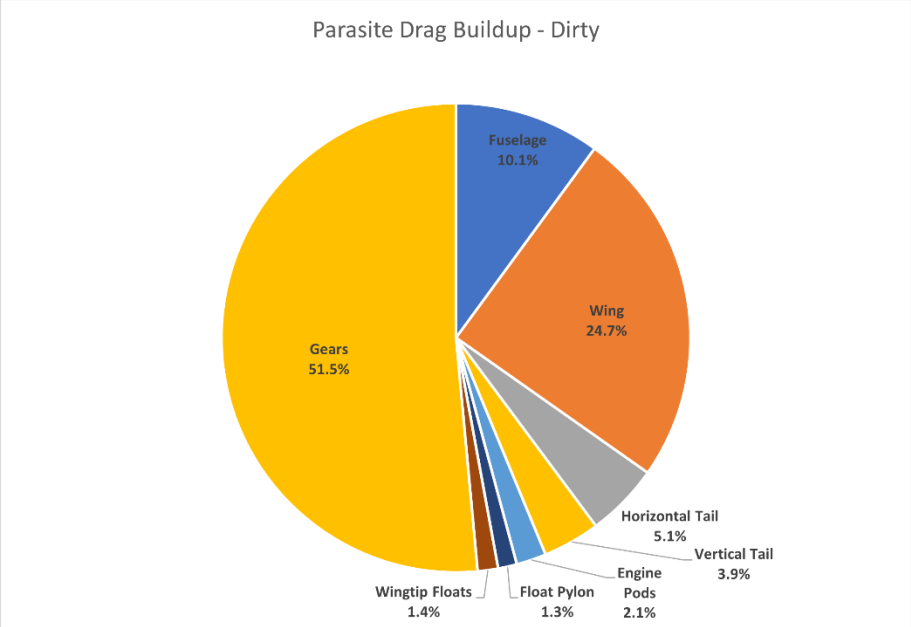

Figure 7.6: Parasite Drag Buildup (Dirty)

Below is a summary of the drag buildup. From Raymer[3], the drag area required to account for base drag and other miscellaneous drags is estimated to be 1.3, and a 10% adjustment for leakage and protuberance drag is added, also suggested in Raymer:

Table 7-3: Parasite Drag Buildup (Clean)

CLEAN	
Component	C_{D_0}
Fuselage	0.0027
Wing	0.0068
Horizontal Tail	0.0014
Vertical Tail	0.0011
Engine Pods	0.0006
Float Pylon	0.0001
Wingtip Floats	0.0004
D/q	1.3
Leakage + Protuberance	10%
TOTAL: **0.0162**	

Table 7-4: Parasite Drag Buildup (Dirty)

DIRTY	
Component	C_{D_0}
Fuselage	0.0028
Wing	0.0069
Horizontal Tail	0.0014
Vertical Tail	0.0011
Engine Pods	0.0006
Float Pylon	0.0004
Wingtip Floats	0.0004
Gears	0.0144
D/q	1.3
Leakage and Protuberance	10%
TOTAL: **0.0329**	

7.6 Induced Drag

It is possible to estimate the induced drag factor K by the following expression:

$$K = \frac{1}{\pi A R e} \qquad 7.9$$

Where e is the Oswald efficiency factor, a parameter that dictates the efficiency of the lift distribution – the closer to the ideal elliptical, the closer to 1.

There are many different empirical methods to estimate e. For subsonic aircraft with less than 30 degrees of leading-edge sweep, the following expression is a reasonable approximation of e:

$$e = 1.78(1 - 0.045A^{0.68}) - 0.64 \qquad 7.10$$

Computing the expressions above yields the following value for the induced drag factor K:

$$K = 0.0421$$

7.7 Ground Effect

As the aircraft approaches the runway, the induced drag can be reduced significantly because of ground effect. Ground effect is the diminishing of the induced downwash angle, therefore reducing induced drag. The effective induced drag factor K_{eff} is given as a function of height above the ground:

$$K_{eff} = \frac{33\left(\frac{h}{b}\right)^{1.5}}{1 + 33\left(\frac{h}{b}\right)^{1.5}} K \qquad 7.11$$

This relationship is plotted below with the previously obtained value of K:

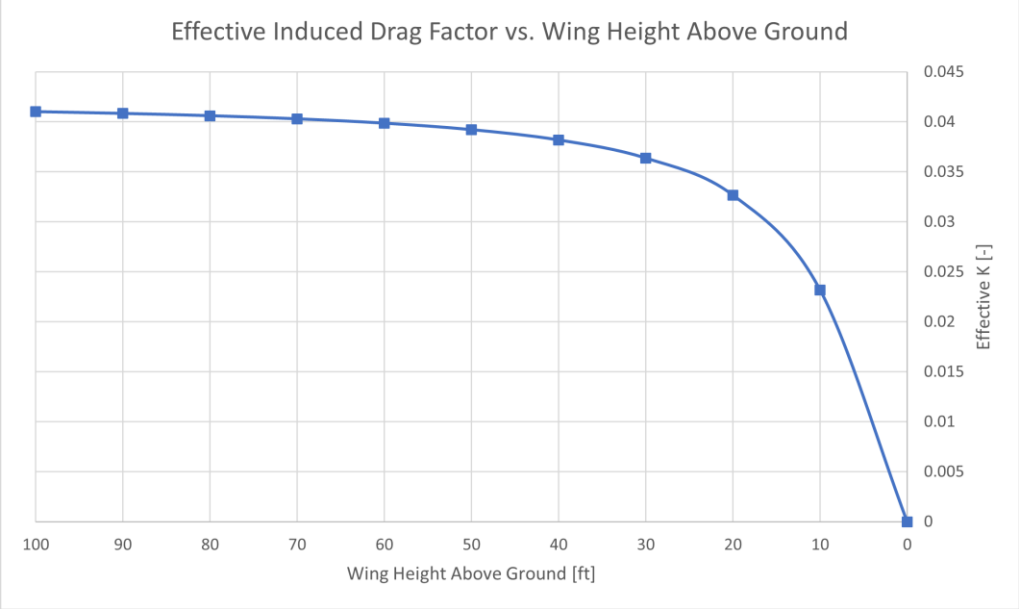

Figure 7.7: K_{eff} versus Wing Height

Chapter 8 – Propulsion

8.1 Overview

Propulsion analysis focuses on the discrepancy between uninstalled and installed thrust as per the methods in Raymer[3]. Uninstalled thrust is estimated based on data from a representative Turboprop. From there, losses in thrust are computed, both from engine-related effects and propeller-related effects.

8.2 Uninstalled Thrust

Uninstalled thrust is the propulsive force obtained by an engine manufacturer's testing prior to installation in an aircraft. Designers must account for disparities between the manufacturer's thrust and the real, experienced thrust with complex aerodynamic effects into play.

This author did not find real engine data for the selected powerplant. Thus, a representative engine is scaled down by power. Raymer presents a representative Turboprop of 6500 horsepower. Its uninstalled thrust was digitized by this author and plotted against Mach number below:

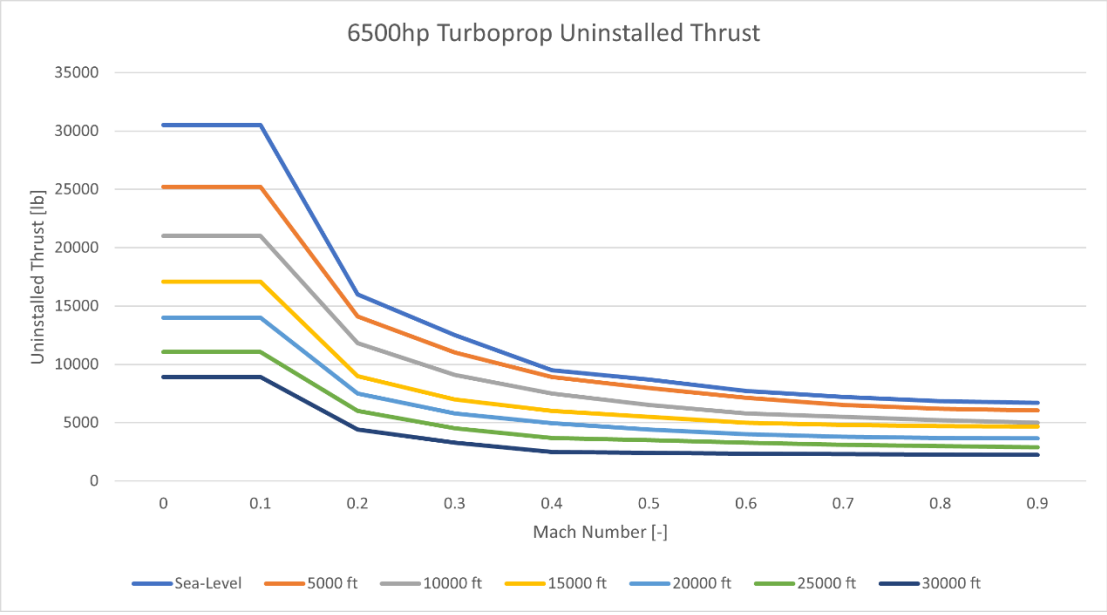

Figure 8.1: Representative Turboprop Uninstalled Thrust

And scaled by power, that is:

$$T_{\text{scaled}} = \left(\frac{P_{\text{AirSChooner}}}{P_{\text{representative}}}\right) T_{\text{representative}} \qquad 8.1$$

The approximately scaled uninstalled thrust can then be plotted versus Mach number like so:

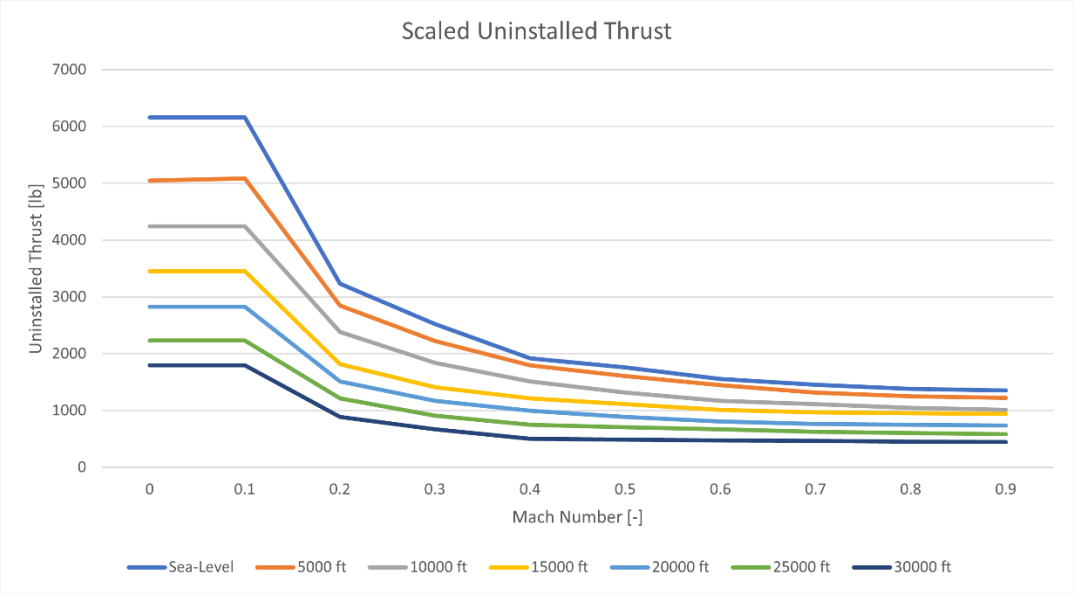

Figure 8.2: Scaled Uninstalled Thrust

Note that the scaling was done for a single engine. Thus, this is the approximate uninstalled thrust for a single engine. To get the total thrust, multiply the values by two.

8.3 Engine-Related Losses

8.3.1 Overview

Raymer[3] describes three main sources of loss in thrust: inlet pressure recovery, bleed air, and horsepower extraction. All of these are described and computed below.

8.3.2 Inlet Pressure Recovery

Inlet pressure recovery losses are thrust losses associated with a disparity between the pressure in the freestream and the pressure in the engine front face. There are also losses associated with pressure drops internal to the inlet duct itself.

In the case of AirSChooner, with a cruising Mach of 0.4, well below the supersonic range, losses due to inlet pressure recovery will not be accounted for. It is hard to estimate exactly what these losses will be given the operating range of the aircraft, and it is safe to assume that the loss will not be significant enough to warrant major design changes in the conceptual level. It is imperative, of course, to conduct thorough thrust testing later in the design process to verify the exact losses.

8.3.3 Bleed Air

Bleed air losses are thrust losses related to the use of part of the air mass flow for other purposes, such as cabin air, anti-icing, and other uses. The thrust loss is more than proportional to the ratio of air bled to total air mass flow. Thus, a constant must correct for this proportionality.

The percent thrust loss due to air bleed is given by:

$$\%T_{\text{air bleed}} = C_{bleed}\left(\frac{\text{bleed mass flow}}{\text{engine mass flow}}\right) \times 100 \qquad 8.2$$

Where C_{bleed} can be approximated as 2 and both the bleed mass flow as well as the engine mass flow are provided by the manufacturer. In case of the representative engine in Raymer's appendix, the percent loss is found to be:

$$\%T_{\text{air bleed}} = 3.8\%$$

8.3.4 Horsepower Extraction

Horsepower extraction losses are thrust losses related to the power used by mechanical components within the engine directly connected to the turbines. These losses are usually given by the manufacturer and, in this case, are present in the appendix of [3].

This representative turboprop has a power extraction of 54kW, or 72.4hp. Scaling this down to this aircraft's engines, the extraction power is found to be:

$$P_{ext} = 14.6 \text{ hp}$$

8.4 Propeller-Related Losses

8.4.1 Cooling Drag

Cooling drag accounts for losses due to the momentum loss of air that is directed over the engine for cooling purposes. It is sensitive to the detail design of the engine and its integration but can be estimated at the conceptual level. Once again, further testing is encouraged.

Cooling drag can be estimated by the expression below:

$$\left.\frac{D}{q}\right)_{\text{cooling}} = 4.9 \times 10^{-7} \frac{bhp\, T^2}{\sigma V} \qquad 8.3$$

Where σ is the density ratio and T is the air temperature. This is estimated and plotted for each combination of Mach and altitude in the last subsection of this chapter.

8.4.2 Miscellaneous Drag

Miscellaneous drag refers to losses due to other components of the engine, such as the oil cooler, exhaust pipes, etc. It is also highly dependent on the detail design of the engine. Miscellaneous drag can be estimated with the expression below:

$$\left.\frac{D}{q}\right)_{\text{misc.}} = (2 \times 10^{-4})bhp \qquad 8.4$$

And is also computed for each Mach and altitude in the following subsection.

8.5 Installed Thrust

Installed thrust can now be estimated by accounting for the previously calculated losses. Percent losses are multiplied by the uninstalled thrust, and drag losses are simply subtracted. The power extraction loss is divided by the velocity to find the thrust loss.

Finally, the installed thrust can be plotted against Mach number for a range of altitudes, as shown below:

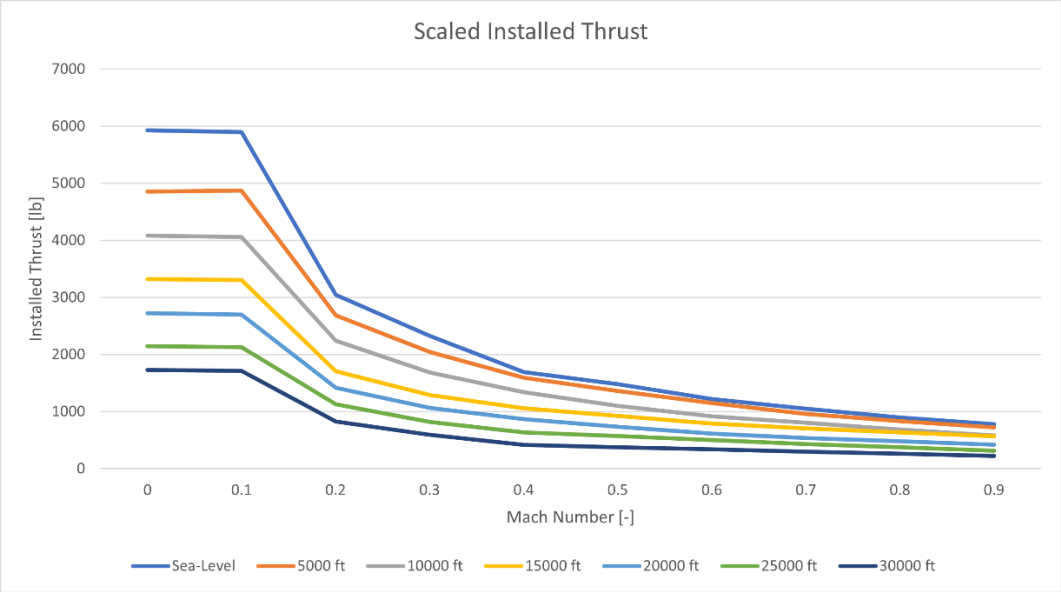

Figure 8.3: Scaled Installed Thrust

Chapter 9 – Structures and Loads

9.1 Material Selection

9.1.1 Wing, Empennage, and Hull

The wing and tail sections of the aircraft must be built in such a way to minimize weight while giving the necessary strength to support the static and airborne loads experienced by these crucial structural components. The hull and its structural components follow the same requirement, with the added concern of water corrosion.

Composites were considered. They offer excellent strength, are lightweight, and offer low manufacturing challenges for experienced manufacturing centers. There are other lightweight, novel options. The use of aluminum-lithium alloys is not unheard of, with some companies reporting weight reductions compared even to composite use.

For the wing, empennage, and hull, composite materials are to be used for their construction. These will be "built-up" elements, with a composite outer skin and metal inner elements – stringers, ribs, and longerons – to save weight and add convenience and strength. Graphite-epoxy and other composite combinations offer great corrosion protection as well, making it suitable for the hull. In fact, the boating industry has long been taking advantage of composite materials, with many boats having a big proportion of their materials be some type of composite.

9.1.2 Wingtip Floats and Pylons

The wingtip floats and its pylons are also of structural concern. The floats must be buoyant and built in such a way to ensure buoyancy, and the pylons must be sound enough to support the compression loads during water landings.

Both the wingtip floats and its pylons are to be constructed of composite materials also. The wingtip floats must have separate, watertight compartments in case of rupture and flooding of one for engineering redundancy. It is also the case that many floats contain pumps that drain the water out of the float, which is often done during pre-flight checks.

9.1.3 Stagnation Temperature and Engine Firewall

During the selection of the above materials, temperature was considered. Supersonic aircraft must choose materials that are temperature resistant, since aerodynamic heating can increase the surface temperature of the aircraft substantially, particularly around sharp corners, such as the nose.

The stagnation temperature can be estimated by the following expression:

$$T_{\text{stag.}} = T_{ambient}(1 + 0.2M^2) \qquad 9.1$$

It can thus be seen that aerodynamic heating is of little concern at AirSChooner's operating envelope, well below the transonic and supersonic ranges.

However, there are locations that require thermal protection. Notably, the engine firewall must resist and dissipate the thermal and oscillatory loads produced by the engine. For these cases, materials like titanium or steel can be used. For this aircraft, steel is selected since it is cheaper than titanium and can be more easily found and manufactured. However, in detail design, dedicated analysis and studies of the required materials for these components must be made.

9.2 V-n Diagram

A V-n diagram shows the flight envelope of the aircraft when it comes to its limitations in speed and load factors. These limitations can be aerodynamic (stall lines) or structural (limit and ultimate load lines.) To construct the V-n diagram, this author used an open-source Python library, ADRpy[8]. The resulting plot is shown below:

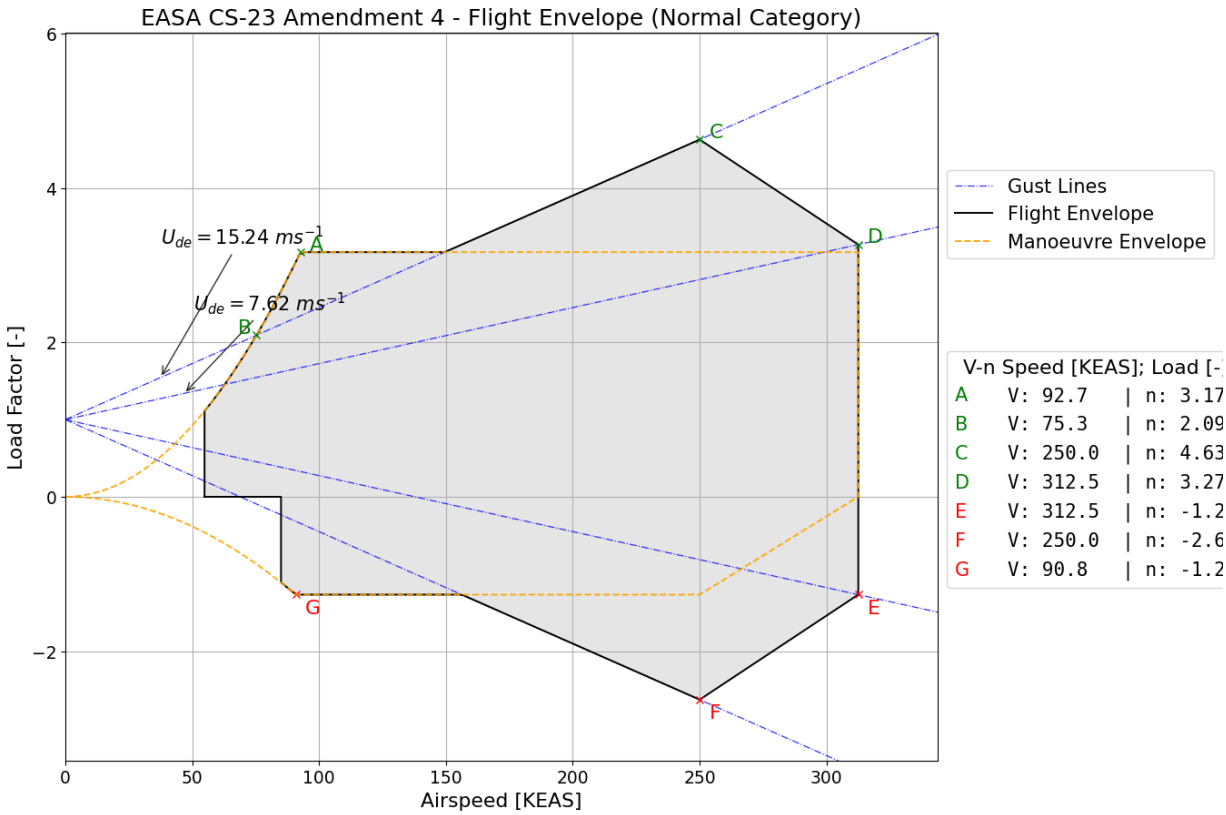

Figure 9.1: AirSChooner V-n Diagram

Where the conversions to knots for both derived gust velocities U_{de} are:

$$U_{de_B} = 29.6 \text{ kts}$$

$$U_{de_D} = 14.8 \text{ kts}$$

The load factors are slightly cropped in the figure, but are shown in the table below:

Table 9-1: Limit Load Factors

Point	n_{lim}
A	3.2
B	2.1
C	4.6
D	3.3
E	-1.2
F	-2.6
G	-1.2

It is worth to note that the derived gust velocities are defined to be the values above. The true gusts experienced are found by taking the product of the derived gust velocity and the gust alleviation factor, K_g:

$$K_g = \frac{0.88\mu_g}{5.3 + \mu_g} \qquad 9.2$$

And μ_g is the mass ratio:

$$\mu_g = \frac{2\left(\frac{W}{S}\right)}{\rho g \bar{c} C_{L_\alpha}} \qquad 9.3$$

These calculations are all internal to the software, so will not be fully developed here. They can be found in detail in [3,4] or other authors.

Chapter 10 – Stability & Control

10.1 Static Stability

10.1.1 AVL Model

To determine whether the aircraft was stable or not, an AVL[9] model of the aircraft was created and the flow conditions were simulated, forcing a straight-and-level condition of trim. It is worth to note that the mass properties of the aircraft, particularly center of gravity location and moments of inertia, are inputs from the user. CG was calculated previously, and moments of inertia were calculated using OpenVSP.

Below are the lattice geometry of the aircraft and Trefftz Plot produced by AVL. A Trefftz plot shows the spanwise lift distribution, with span location on the horizontal axis and normalized coefficient of lift on the vertical axis. Though more related to aerodynamics, the Trefftz plot confirms our aerodynamic results, with a remarkably close value to the Oswald Efficiency factor obtained previously:

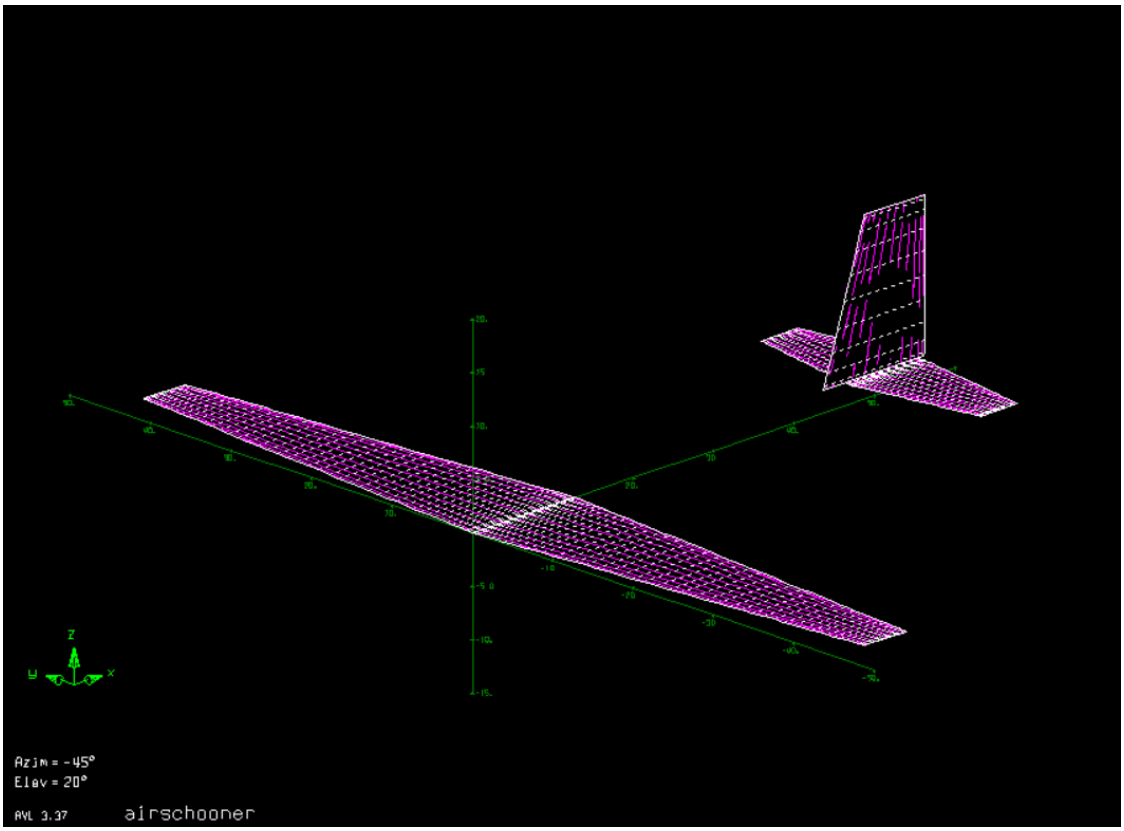

Figure 10.1: AVL AirSChooner Model

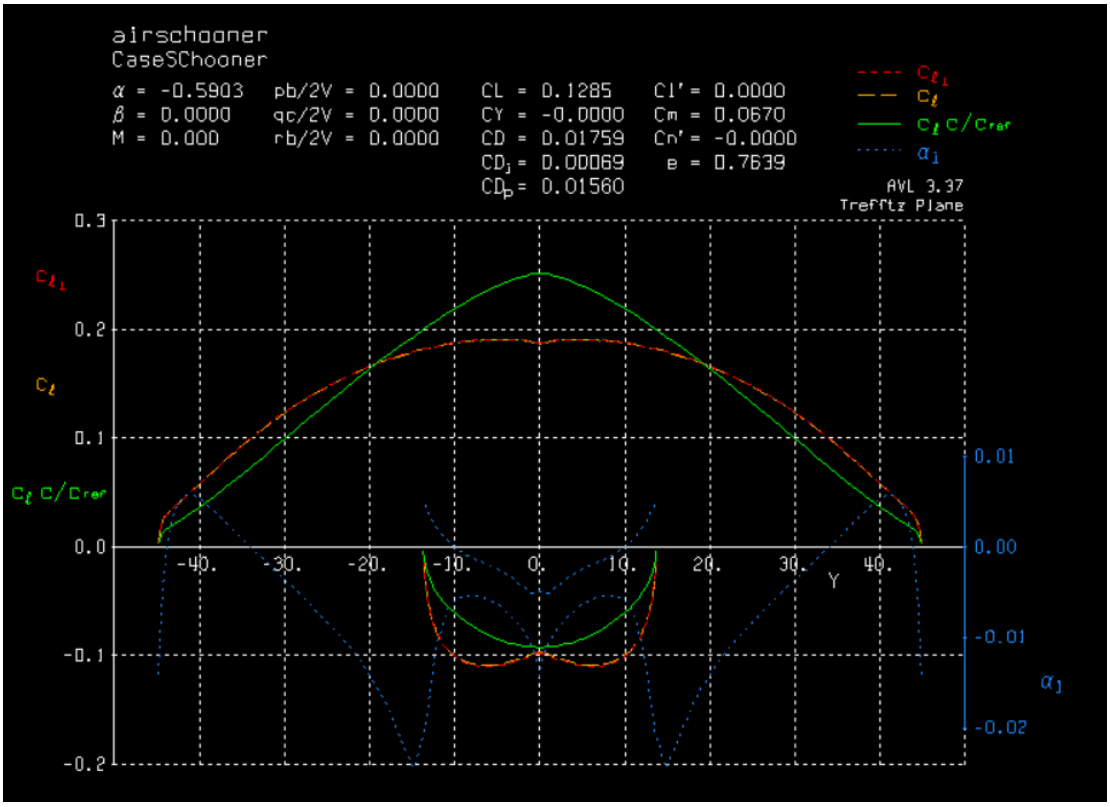

Figure 10.2: AVL AirSChooner Trefftz Plot

The fuselage was not modeled in AVL. Panel and vortex codes are known to not model the aerodynamics of wing-fuselage and tail-fuselage interactions accurately. Because of that, and given a relatively nominal aerodynamic operation – well below supersonic – it is safe to assume that these interactions will not affect the stability significantly.

10.1.2 Stability Derivatives

With AVL, we can verify the stability derivates, that is, variations in pitching, rolling, and yawing moments with respect to variations in angle of attack and angle of sideslip.

Below is a table that summarizes the results, taken directly from AVL:

Table 10-1: Stability Derivatives

Stability Derivative	C_{m_α}	C_{l_β}	C_{n_β}
Requirement	**Negative**	**Negative**	**Positive**
Result	-1.42	-0.04	0.18
Meets Requirement?	**YES**	**YES**	**YES**

The stability derivatives show the static stability, both longitudinal and lateral, of the aircraft. Furthermore, the neutral point is calculated in AVL as:

$$X_{np} = 25.8 \text{ ft}$$

The neutral point is aft of the center of gravity, a good indication of stability. Furthermore, all stability derivatives indicate static stability. Note that the convention for C_{n_β} to positive instead of the usual negative. This follows the "trailing edge down" convention for stability analysis.

10.2 Variation of Aerodynamic Center with Mach Number

It is useful to analyze the change in stability with changes in flow conditions. Namely, the aerodynamic center of the aircraft is closely related to Mach number, which can have important stability implications. The famous Mach tuck, for instance, an aerodynamic effect that creates a tendency for the aircraft to pitch down in the transonic/supersonic regions, has claimed lives.

The change in the aerodynamic center of the aircraft against Mach number can be modeled by the following expression:

$$x_{ac} = x_{c/4} + \Delta x_{ac}\sqrt{S_{wing}} \qquad 10.1$$

Where the change in aerodynamic center, Δx_{ac}, is given by:

$$\Delta x_{ac} = 0.26(M - 0.4)^{2.5} \qquad 10.2$$

For a subsonic/lower supersonic range of Mach numbers. This can then be plotted against Mach number:

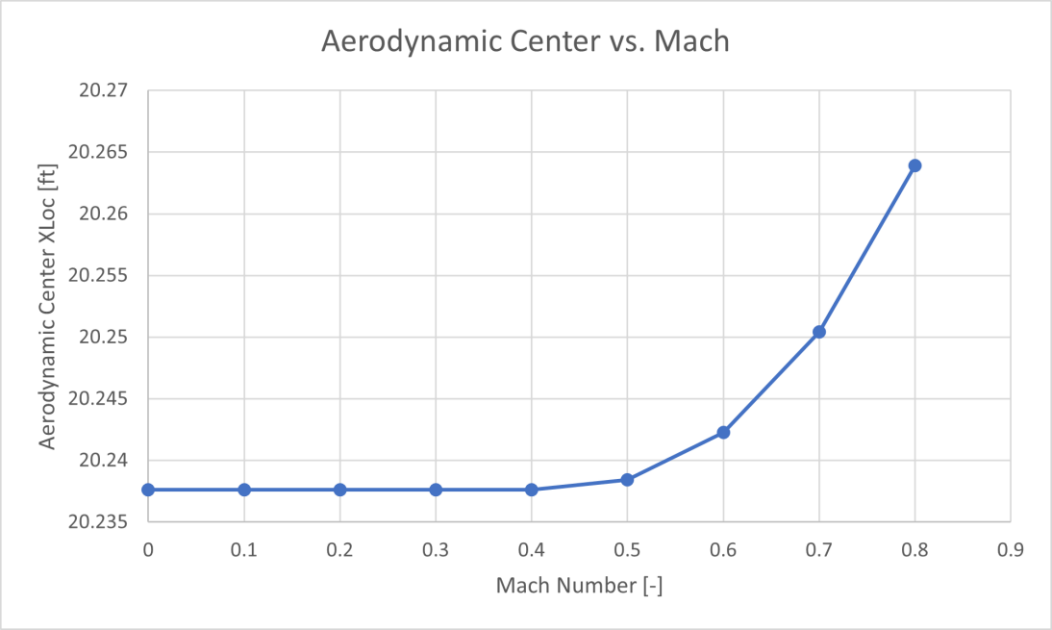

Figure 10.3: Aerodynamic Center versus Mach Number

As can be seen, the change in longitudinal location is not significant for the operating range of the aircraft. It starts to become significant near the transonic and supersonic range, which is not in the operating envelope of this aircraft. These results indicate the stability of AirSChooner.

Chapter 11 – Cost Analysis

11.1 DAPCA IV Model

Cost analysis was conducted following the RAND DAPCA IV model. This is a cost-estimating relationship (CER) that aims to estimate different costs during the development and construction of novel aircraft as a function of empty weight, maximum velocity, production quantity, and other miscellaneous variables.

These equations are omitted from this report but are laid out in [3]. Below, the results will be presented with and without the cost of engine production, since engine selection and testing is hard to predict, and depends deeply on each customer and how they would purchase AirSChooner. Any other assumptions and corrections are explicitly stated below.

11.2 Research, Development, Test, and Evaluation (RDT&E) and Flyaway Costs

RDT&E includes all the engineering work done on an aircraft. That is, it includes all stages of design, development, prototyping, flight test, and even certification costs. It does not include the costs of ground handling of the aircraft, maintenance, fuel, insurance, etc.

Flyaway – or "production" – costs include the labor, materials, and facilities required to manufacture the aircraft. The cost of avionics is included in the flyaway cost. This is dependent on how many aircraft are being manufactured, and the cost tends to decrease as more aircraft are manufactured due to what is called the learning curve effect. Early in manufacturing, the exact tooling and production lines are not fully designed and optimized. However, with more and more units, production becomes "easier" as manufacturers "learn" how to optimally produce the aircraft.

Below are two pie charts representing the RDT&E and flyaway costs, with and without accounting for engine production. Neither of these accounts for avionics, a constant in the calculations:

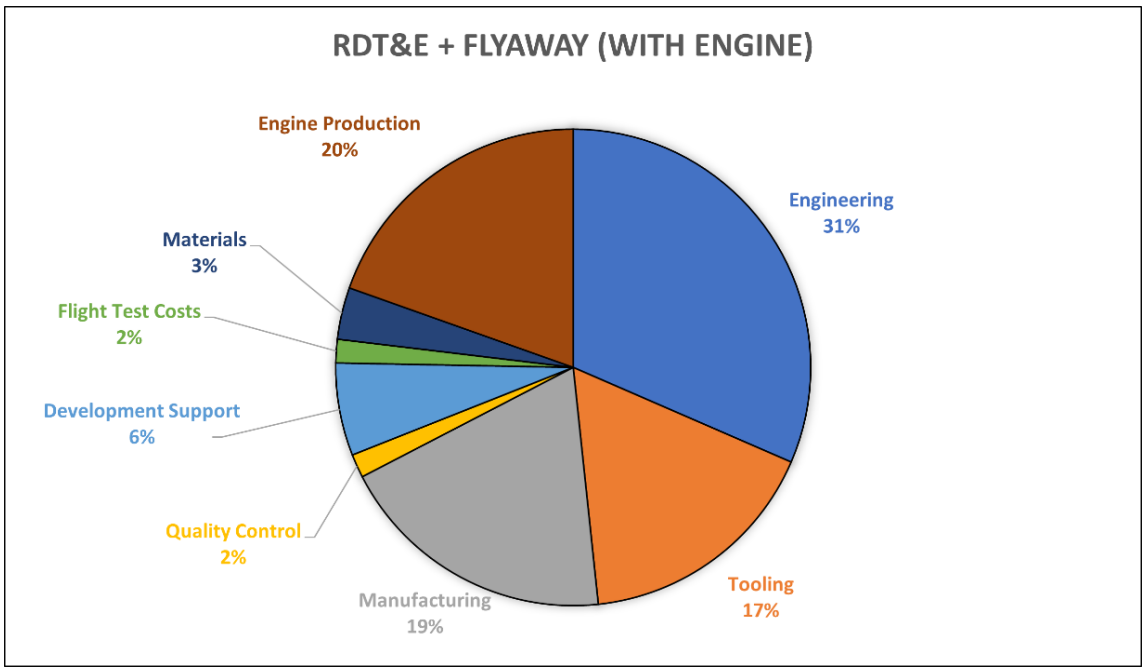

Figure 11.1: RDT&E + Flyaway (With Engine)

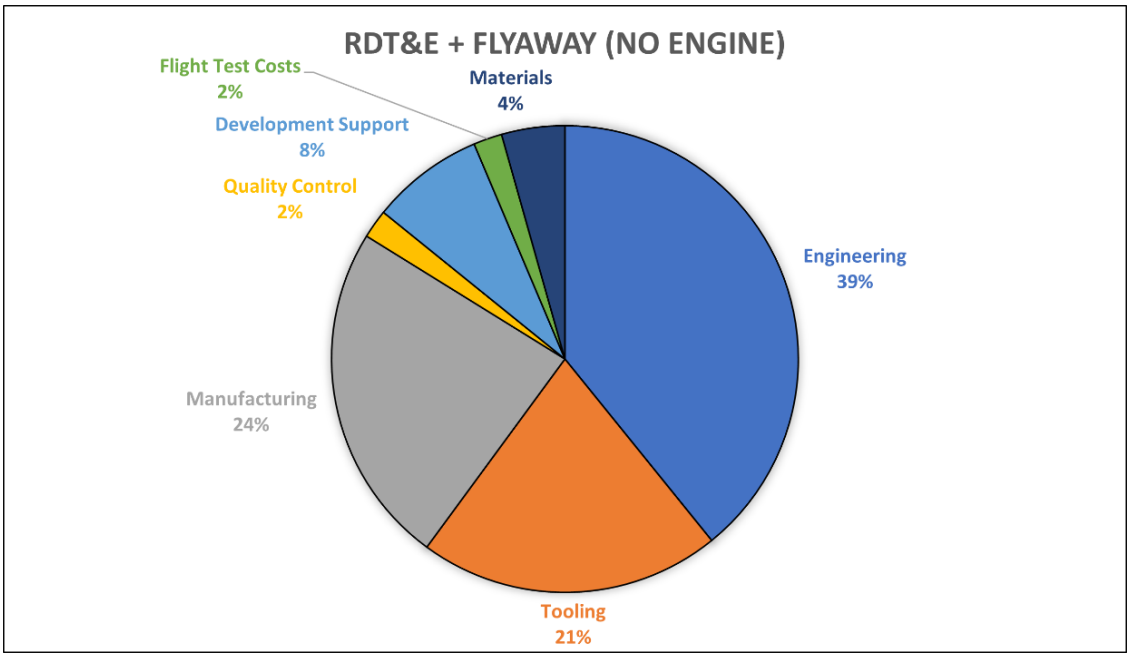

Figure 11.2: RDT&E + Flyaway (No Engine)

And a table below summarizes the costs with and without engine production costs:

Table 11-1: RDT&E + Flyaway Summary

Category	Cost
Engineering	$229,999,721
Tooling	$122,718,463
Manufacturing	$139,414,091
Quality Control	$11,676,641
Development Support	$45,908,830
Flight Test Costs	$11,641,653
Materials	$25,717,345
Engine Production	$142,988,493
TOTAL (ENGINE)	**$730,065,237**
TOTAL (NO ENGINE)	**$587,076,744**

All hourly rates used to arrive at the engineering, tooling, manufacturing, and quality control costs were factored by inflation following the Consumer Price Index (CPI). Finally, all numbers above assume an initial production of 10 aircraft, as well as 2 test flight aircraft.

11.3 Operations and Maintenance (O&M) Costs

11.3.1 Fuel and Oil Costs

Yearly fuel costs per aircraft can be estimated with the following expression:

$$C_f = (C_{bhp})(P)\left(\frac{FH}{Y}\right)\left(\frac{C_f}{lb}\right) \qquad 11.1$$

In other words, the cost of fuel per year per aircraft is equal to the product of the brake-specific fuel consumption, brake horsepower, flight hours per year per aircraft, and the cost of fuel by the pound.

Computing these values for a typical yearly flight time of 2500 hours per aircraft and adjusting the fuel prices for inflation, the following is an estimated yearly fuel cost:

$$C_f \approx \$3{,}368{,}057 \frac{1}{(YR)(AC)}$$

The cost of oil is negligible when compared to the cost of fuel, so can be ignored for this initial analysis.

11.3.2 Crew Salaries

Crew cost per block hour can also be estimated through the use of statistical equations. Block hours are the total operation time of an aircraft's mission, from the time the blocks are removed from the wheels to the time they are placed back on the aircraft at the destination. The equation is shown below:

$$C_c = 94.5\left(V\frac{W_0}{10^5}\right)^{0.3} + 237.2 \qquad 11.2$$

Where V is the cruise velocity. Computing this yields the following value for crew cost per block hour:

$$C_c \approx \$551$$

This value is just an approximation and, as stated in Raymer, crew costs vary wildly nowadays from airline to airline.

Chapter 12 – Design Summary and Three-View Diagrams

12.1 Design Summary

A design was presented for an aircraft with the following geometric characteristics:

Table 12-1: AirSChooner Design Summary: Geometry

	Geometry	Value
Wing	Aspect Ratio (AR)	10
	Wing Area (S)	804.1 ft^2
	Wingspan (b)	89.7 ft
	MAC (c)	9.5 ft
	Taper Ratio (λ)	0.4
	LE Sweep Angle ($\Lambda_{L.E.}$)	5 deg
Horizontal	Aspect Ratio (AR)	4
	Wing Area (S)	187.3 ft^2
	Wingspan (b)	27.4 ft
	MAC (c)	7.1 ft
Vertical	Aspect Ratio (AR)	1.5
	Wing Area (S)	151.3 ft^2
	Wingspan (b)	15.1 ft
	MAC (c)	10.3 ft
Fuselage	Length (L_f)	57.2 ft
	Max Beam (B_f)	80 in
	Max Height (H_f)	100 in
	Fineness Ratio (f)	6.9

And the following weight/power characteristics:

Table 12-2: AirSChooner Design Summary: Weights and Power

Characteristic	Value
Wing Loading	27.2 lb/ft^2
Power-to-Weight Ratio	0.12 hp/lb
V_{max}	250 kts
$P_{each\ engine}$	1312 hp
W_0 Passenger	21619 lbs
W_0 Cargo	21872 lbs
W_0 Economic	21032 lbs

12.2 Additional Operational Considerations

There are some additional considerations to be made about the operational aspects of the aircraft.

The aircraft was primarily constrained by the passenger mission in layout and cargo mission in weight/sizing. However, the aircraft designed is the same when it comes to its empty weight. The customer will have a say on whether to operate a passenger-configured aircraft or a cargo-configured aircraft. All passenger seats are installed in a moving rail setting, where the conversion from passenger to cargo and vice-versa is possible with moderate to low logistical/operational capabilities.

Furthermore, operation of the aircraft is possible even when low operational capabilities are available. The high-wing configuration allows for loading/unloading of cargo in doors located close to the ground on the right-hand side of the aircraft, as shown below:

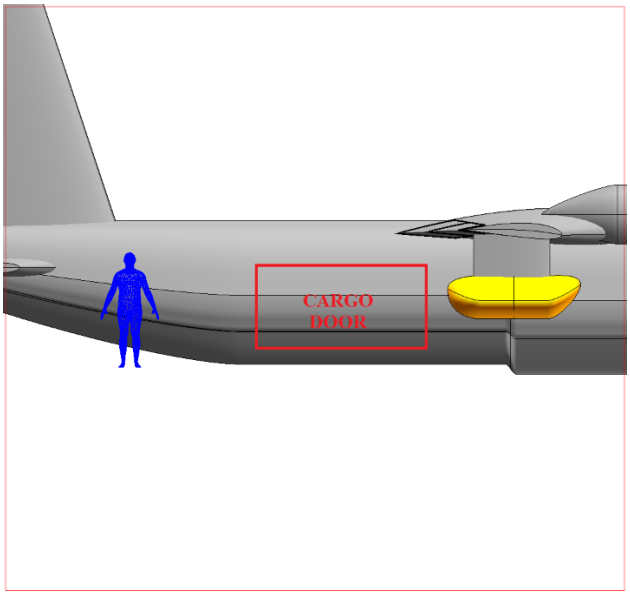

Figure 12.1: Cargo Loading/Unloading Door (Human for Scale)

12.3 Three-View Dimensioned Drawings

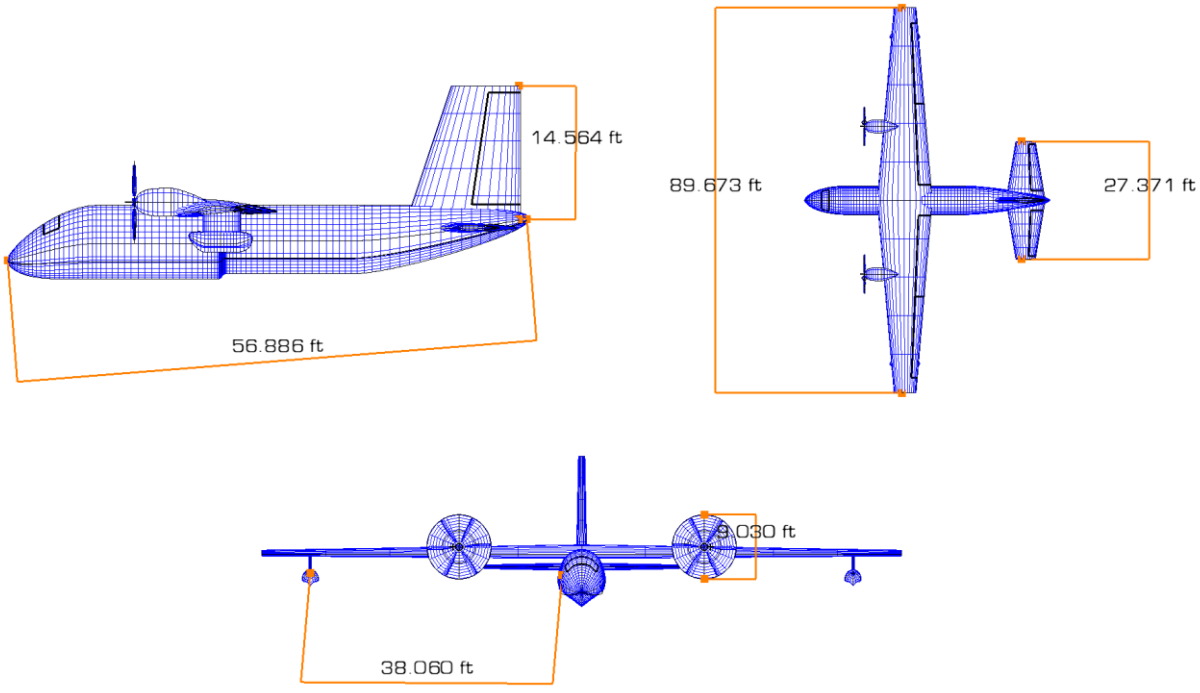

Figure 12.2: Three-View Dimensioned Drawing

Chapter 13 – References

[1] AIAA, *Undergraduate Individual Aircraft Design RFP – New Efficient Water and Terrestrial (NEWT) Aircraft*, https://www.aiaa.org/get-involved/students-educators/Design-Competitions, 2023.

[2] Jane, Fred T., *Jane's All the World's Aircraft: Development and Production*, 1973-2010.

[3] Raymer, D. P., *Aircraft Design: A Conceptual Approach*, 6th ed., American Institute of Aeronautics and Astronautics, 2018.

[4] Roskam, J., *Airplane Design Parts I-VIII*, DARcorporation, Lawrence, KS, 2018.

[5] Drela, M., *XFOIL: An Analysis and Design System for Low Reynolds Number Airfoils*, Conference on Low Reynolds Number Airfoil Aerodynamics, University of Notre-Dame, June 1989.

[6] Gudmundsson, S., *General Aviation Aircraft Design: Applied Methods and Procedures*, Butterworth-Heinemann, 2013.

[7] McDonald, Robert A. and Gloudemans, James R., *Open Vehicle Sketch Pad: An Open Source Parametric Geometry and Analysis Tool for Conceptual Aircraft Design*, AIAA 2022-0004. AIAA SCITECH 2022 Forum. January 2022.

[8] Sobester, A., *ADRpy*, https://github.com/sobester/ADRpy

[9] Drela, M. and Youngren, H., *AVL (3.30) User Primer, AVL Overview*, http://web.mit.edu/drela/Public/web/avl/avl_doc.txt